



Contents lists available at ScienceDirect



Combined effects of humic substances and clay minerals on U(VI) bioreduction



Yu Chen ^{a,b}, Limin Zhang ^{a,c}, Shuaidi Wang ^{a,d}, Qiang Zeng ^{a,d}, Qingyin Xia ^{a,d}, Runjie Li ^a, Dongyi Guo ^{a,d}, Zezhen Pan ^e, Hailiang Dong ^{a,d,*}

^a Center for Geomicrobiology and Biogeochemistry Research, State Key Laboratory of Biology and Environmental Geology, China University of Geosciences, Beijing 100083, China

^b School of Water Resources and Environment, China University of Geosciences, Beijing 100083, China

^c State Key Laboratory of Microbial Resources, Institute of Microbiology, Chinese Academy of Sciences, Beijing 100101, China

^d School of Earth Sciences and Resources, China University of Geosciences, Beijing 100083, China

^e Department of Environmental Science and Engineering, Fudan University, Shanghai 200438, China

ARTICLE INFO

Article history:

Received 5 June 2022

Accepted 14 October 2022

Available online 20 October 2022

Associate editor: Christophe Tournassat

Keywords:

U(VI) reduction

Clay minerals

Humic substances

U(IV) speciation

ABSTRACT

In the last several decades, microbial reduction of U(VI) to U(IV) has been applied as a method to remediate uranium contamination *in situ*. The U(VI) bioreduction kinetics and resulting U(IV) speciation are affected by various environmental factors, such as humic substances (HS) and Fe-bearing clay minerals. Previous studies have largely focused on their individual effects on U(VI) bioreduction. However, HS and Fe(III)-bearing clay minerals often co-exist at uranium contaminated sites, their joint effects may be different from the sum of their individual ones, due to either synergistic or antagonistic interactions between the two. In this work, we investigated the combined effects of HS and Fe(III)-bearing clay minerals (Fe-rich nontronite and Fe-poor montmorillonite) on U(VI) reduction by *Shewanella putrefaciens* and the resulting U(IV) speciation. HS alone exhibited an inhibitory effect on U(VI) bioreduction, likely because HS retained a fraction of electrons from microbial oxidation of lactate. The resulting U(IV) was in the form of aqueous U(IV)-HS complex. Clay minerals alone also inhibited U(VI) bioreduction because a fraction of reduced U(IV) was likely re-oxidized by structural Fe(III) and thus electrons were partially diverged from U(VI) to structural Fe(III). Bioreduced U(IV) was in a solid phase. However, in the presence of both HS and clay minerals, their combined effect of inhibition on U(VI) bioreduction was not a simple addition of the two individual ones. In the co-presence of clay minerals and a low concentration of HS (10 and 20 mg C/L), their combined inhibition effect on U(VI) bioreduction was stronger than that of HS but weaker than that of clays. The stronger inhibition than that of HS alone was due to electron diversion by clay minerals. The weaker inhibition than that of clays alone was because HS and/or Fe(III)-HS/Fe(II)-HS served as electron shuttles to accelerate the rate of Fe(III) reduction. These double shuttles decreased the ability of structural Fe(III) in clays to diverge electrons from U(VI) and thus partially negated the inhibitory effect of clay minerals. In the co-presence of clay minerals and a high concentration of HS (100 mg C/L), their combined effect on U(VI) bioreduction was initially similar to that in the low concentration of HS scenario. However, over extended time, clay minerals partially negated the inhibitory effect of HS, likely because clay minerals adsorbed a fraction of HS and thus lowered the ability of residual aqueous HS to retain electrons. Biogenic U(IV) was sequestered in solid in the presence of Fe-rich nontronite and HS but partially remained soluble in the presence of Fe-poor montmorillonite and HS. This study highlights the importance of the complex interaction between HS and Fe-bearing clays in bioreduction of U(VI) and speciation of the resulting U(IV).

© 2022 Elsevier Ltd. All rights reserved.

1. Introduction

Uranium, a natural nuclear fuel material, is widely used in the nuclear industry. The large-scale mining of uranium ore deposits and inappropriate disposal of nuclear wastes have led to uranium contamination in the environment (Campbell et al., 2015;

* Corresponding author at: Center for Geomicrobiology and Biogeochemistry Research, State Key Laboratory of Biology and Environmental Geology, China University of Geosciences, Beijing 100083, China.

E-mail address: dongh@cugb.edu.cn (H. Dong).

Dewar, 2019; Xia et al., 2020; Cui et al., 2022). Uranium has two major oxidation states, hexavalent uranium [U(VI)] under oxidizing conditions and tetravalent uranium [U(IV)] under reducing conditions (Alessi et al., 2012; Bargar et al., 2013; Alessi et al., 2014; Cui et al., 2022). Reduction of soluble U(VI) to less soluble U(IV) through biotic and/or abiotic processes is considered as an efficient strategy to immobilize U(VI) contamination and minimize its environmental impact.

U(VI) bioreduction is affected by environmental conditions (Cui et al., 2022), such as calcium (Brooks et al., 2003), nickel (Gu et al., 2005), nitrate (Istok et al., 2004), Fe(III)-bearing minerals (Zhang et al., 2009), and humic substances (Gu et al., 2005; Burgos et al., 2007). The resulting U(IV) exists as either insoluble uraninite, fairly mobile amorphous U(IV), monomeric U(IV) or ligand-complexed aqueous U(IV) [such as citrate/EDTA/HS-complexed U(IV)] (Luo and Gu, 2009; Fletcher et al., 2010; Sharp et al., 2011; Alessi et al., 2012; Morin et al., 2016; Bone et al., 2017; Zhang et al., 2021). Therefore, understanding the biogeochemistry of uranium under environmentally relevant conditions provides better insights into the development of bioremediation strategies of uranium contamination.

Fe-bearing clay minerals are ubiquitous in soil and sediments, and are often used as nuclear waste disposal barriers because of their high adsorption capacity and low hydraulic conductivity (Sellin and Leupin, 2013). The associated Fe(II)/Fe(III) couple in Fe-bearing clay minerals is redox-active and participates in the transformation of contaminants such as nitrate (Zhao et al., 2015), chromium (Liu et al., 2019), and uranium (Zhang et al., 2009, 2021; Satpathy et al., 2022; Xia et al., 2022). U(VI) can be reduced by Fe(II) in chemically reduced smectite, which decreases the mobility of uranium in the environment (Satpathy et al., 2022). Opposite to the reductive role of Fe(II), Fe(III) in oxidized clay minerals can serve as an oxidant to oxidize biogenic U(IV) (Zhang et al., 2009, 2011; Xia et al., 2022), which may remobilize previously precipitated U(IV) (Zhang et al., 2011). Therefore, Fe-bearing clay minerals play important roles in the uranium biogeochemistry and the bioremediation of uranium contamination.

Humic substances (HS) make up a significant fraction of natural organic matter in terrestrial and aquatic environments (Olk et al., 2019). HS are known to co-exist with clay minerals at uranium contaminated sites (Wang et al., 2013; Bone et al., 2017, 2020; Fuller et al., 2020), which significantly increase the complexity of biogeochemical cycling of uranium. HS contain redox-active functional groups such as quinone moieties, which can accept electrons from microbial respiration (Scott et al., 1998; Aeschbacher et al., 2010; Klüpfel et al., 2014). Reduced HS can then transfer electrons to redox-active metals such as structural Fe(III) in minerals and Cr (VI) (Liu et al., 2017; Mohamed et al., 2020), and thus impact the biogeochemistry of these metals. For uranium, HS can not only change the bioreduction rate of U(VI) (Gu and Chen, 2003; Gu et al., 2005; Burgos et al., 2007), but also chelate with bioreduced U(IV) (Burgos et al., 2007; Luo and Gu, 2009) to form aqueous U (IV)-HS complex (Gu et al., 2005), thus impacting the fate and transport of U(IV). In natural environments, HS may partially sorb onto clay minerals, which results in fractionation of HS into aqueous and sorbed forms (Ghosh et al., 2009; Zhang et al., 2012). The electron transfer capacity of residual aqueous fraction of HS may be different from that of original HS (Ghosh et al., 2009). Meanwhile, the sorbed fraction of HS may modify the surface properties of clay minerals (Ghosh et al., 2009) and therefore may impact the redox reactivity of clay minerals (Liu et al., 2017). These complex interactions between HS and clay minerals may significantly affect the bioreduction of uranium, but such impacts have largely remained unknown.

To date, previous studies have only investigated the combined effects of clay minerals and anthraquinone-2,6-disulfonate (AQDS)

or small organic ligands such as citrate on the bioreduction of U (VI). AQDS serves as a redox-active analogue of HS (Zhang et al., 2009) and citrate contains metal chelating functional groups that are similar to those of HS (Gu et al., 2005; Zhang et al., 2021). However, HS are polyfunctional, polyelectrolytic, and heterogeneous mixtures of organic molecules, and the ability to transfer electrons and chelate metals are much more complex than those of either AQDS (Gescher and Kappler, 2013; Liu et al., 2017) or citrate (Cumberland et al., 2016). A recent study demonstrated that AQDS cannot fully represent the effect of HS on the bioreduction of Fe(III) in clay minerals, because of the complex composition of HS (Liu et al., 2017). More importantly, AQDS is a synthetic analogue of HS and is often used in the laboratory to simulate the effect of HS (Zhang et al., 2009) and organic ligands such as citrate and EDTA are only present at certain uranium contaminated sites (Francis and Dodge, 2008; Stewart et al., 2013; Xia et al., 2022). Therefore, their impacts cannot be extrapolated to environmentally more complex organic matter in general. Therefore, it is important to understand the combined effects of HS and Fe(III)-bearing clay minerals on U(VI) bioreduction and the resulting U (IV) speciation.

To answer these questions, two well-studied HS (peat humic acid and Suwannee River fulvic acid) (Ratasuk and Nanny, 2007; Aeschbacher et al., 2010; Klüpfel et al., 2014) and two clay minerals (Fe-rich nontronite and Fe-poor montmorillonite) (Bishop et al., 2011; Gorski et al., 2013) were selected in this study. A model bacterium of dissimilatory metal-reducing bacteria (DMRB), *Shewanella putrefaciens* strain CN32, was used to catalyze U(VI) bioreduction under neutral pH and anoxic conditions. We hypothesize that the combined effects of HS and clay minerals on U(VI) bioreduction is either synergistic or antagonistic, rather than the simple sum of their individual ones. The following questions are addressed: (1) what are the combined effects of HS and Fe-bearing minerals on the U(VI) bioreduction kinetics and the resulting U(IV) speciation, relative to their individual impacts? (2) What are the underlying mechanisms of U(VI) bioreduction in the presence of both HS and clay minerals? The results of this study provide new knowledge of uranium biogeochemical transformations in a complex system and have important implications for uranium bioremediation.

2. Materials and methods

2.1. Chemicals, clay minerals, and humic substances

All chemicals used in the experiments were of analytical reagent grade. Water was obtained from a Milli-Q reference ultraviolet (UV)-water system (MQ-H₂O). Uranyl acetate and sodium lactate were dissolved in anoxic and sterile buffer of 30 mM bicarbonate (NaHCO₃) and 10 mM PIPES solutions (hereafter referred to as BP buffer, pH 7), and filtered through 0.22 μm nylon filters to obtain 10 mM U(VI) and 100 mM sodium lactate stock solutions.

Nontronite (NAu-2), montmorillonite (SWy-2), and kaolinite (KGa-1) were purchased from the Source Clays Repository of the Clay Minerals Society (West Lafayette, Indiana, US). The reported formulas of NAu-2 and SWy-2 are (K_{0.01}Na_{0.30}Ca_{0.15})_{(Al_{0.55}Fe²⁺_{0.06}Fe_{3.27}Mg_{0.12})_{(Si_{7.57}Al_{0.15}Fe³⁺_{0.28})O₂₀(OH)₄} and (K_{0.16}Na_{0.19}Ca_{0.02})_{(Al_{3.29}Fe²⁺_{0.01}Fe³⁺_{0.34}Mg_{0.28})_{(Si_{7.90}Al_{0.10})O₂₀(OH)₄}, respectively (Bishop et al., 2011). NAu-2 is an iron-rich smectite with 21.2 wt% Fe content, 97 % of which is Fe(III). SWy-2 is an iron-poor smectite containing only 2.3 wt% Fe, and 98 % of which is Fe(III) (Zeng et al., 2019, 2020a). Manually ground NAu-2 and SWy-2 samples were suspended in 500 mM NaCl for 24 h to achieve Na⁺ homogenization (Zeng et al., 2017). Specific size fraction (<2 μm) was}}

collected by repeated centrifugation and re-suspension (Zeng et al., 2020b). Clay mineral stock solutions (10 g/L) were prepared in BP buffer in serum bottles, sealed with a butyl rubber septum, purged with N₂:CO₂ (80:20 vol ratio), and autoclaved (121 °C for 20 min). KGa-1 is an Fe-poor kaolinite containing only 0.10–0.45 wt% Fe (Zhang et al., 2021).

Two humic substances (HS), peat humic acid (HA) and Suwannee River fulvic acid (FA) were purchased from the International Humic Substances Society (IHSS) (Ratasuk and Nanny, 2007). HA and FA were extracted from peat and river water, respectively (Thurman and Malcolm, 1981). HA and FA were dissolved into BP buffer, stirred for 12 h, and filtered through 0.45 µm acetate cellulose membrane filters. The filtered suspensions were deoxygenated by purging with a gassing station (N₂:CO₂ 80:20) and pasteurized in 70 °C water bath for 30 min, which does not change the properties of HS (Kolokassidou et al., 2007), and stored at 4 °C in the dark until use. Dissolved organic carbon (DOC) of HA and FA stock solutions, determined with an Analytik-jena multi N/C 2100 s series analyzer (Zeng et al., 2020a), was 1035 and 365 mg C/L (referred to as ppm hereafter), respectively.

2.2. U(VI) adsorption to clay minerals

A previous study showed that U(VI) could be adsorbed by NAu-2 (Zhang et al., 2009), which may impact the kinetics of U(VI) bioreduction. To test the ability of clay minerals to adsorb U(VI) under the experimental conditions, control experiments were conducted. Uranium acetate stock solution was added to 2 g/L NAu-2 or SWy-2 suspension to reach the final concentration of 0.5 mM in the absence or presence of 100 ppm HA in BP buffer. At selected time points, 0.2 mL sample was collected, centrifuged (10,000g, 10 min), and filtered (0.22 µm, nylon). The filtrate was used to measure U(VI) concentration by using the Arsenazo III method (see Section 2.7 for methods). The amount of U(VI) adsorbed to clay minerals was calculated from the difference between the initial U (VI) concentration added to the system and U(VI) concentration at specific time points.

2.3. Uranium bioreduction in the presence of humic substances and clay minerals

Shewanella putrefaciens strain CN32 was used for U(VI) reduction experiments, which has the ability to reduce U(VI) (Luan et al., 2014) and to use HS as either electron acceptor, donor, or shuttle (Royer et al., 2002a, 2002b; Chen et al., 2003; Gu and Chen, 2003). CN32 cells were cultured aerobically for 16 h in Luria-Bertani (LB) medium at 25 °C on an orbital shaker. The cells were harvested at the exponential growth phase by centrifugation (3000g, 4 °C, 5 min) and washed three times using deoxygenated and sterilized BP buffer. Cell pellets were resuspended in the same buffer to a concentration of ~ 1.5 × 10⁹ cells/mL as stock culture. The optical density was measured using a UV-vis spectrophotometer (UV-2550, SHIMADZU) at 600 nm. BP buffer, sodium lactate, clay mineral, uranyl acetate, HS, and CN32 were added to 30-mL Balch tubes to start the bioreduction experiments (Table S1). Lactate served as the sole electron donor, and its final concentration was 10 mM. The final concentrations of cell and U(VI) were ~ 1.5 × 10⁸ cells/mL and 0.5 mM, respectively. A relatively higher concentration of U(VI), which was within or near the upper end of the concentration range of U(VI) at contaminated sites (Regenspurg et al., 2010; Luo and Gu, 2011; Bargar et al., 2013; Long et al., 2015; Cui et al., 2022), was chosen to study the kinetics of U(VI) bioreduction. A concentration gradient of HA (10, 20, and 100 ppm) was used either alone or in combination with NAu-2 or SWy-2 (2 g/L concentration). These concentrations of HS, which are within the concentration range of HS in soils and sediments (Zeng

et al., 2020b), were widely used in previous studies that simulated uranium contaminated environments (Gu and Chen, 2003; Gu et al., 2005; Tinnacher et al., 2013). In some experiments HA was replaced by either FA or 0.1 mM (~40 ppm) AQDS. Abiotic, no-HS, and no-clay controls were set up (Table S1). The total reaction volume was 15 mL, and sample tubes were crimp-sealed with rubber stoppers. All experiments were set up in triplicate inside an anoxic chamber (5 % H₂ and 95 % N₂, Coy Laboratory Products, Grass Lake, MI, USA) at room temperature (25 °C). The pH values remained at 7.0 ± 0.1 by the end of all reactions.

2.4. Experiments testing HA as an electron shuttle to accelerate U(VI) and NAu-2 bioreduction

Control experiments were performed to test the ability of HA to serve as an electron shuttle to accelerate U(VI) and Fe(III) bioreduction. First, 200 ppm HA was bioreduced by CN32 in BP buffer for 12 h, and the resultant reduced HA (rHA) solution was sterilized by passing through a 0.22 µm filter (Lovley et al., 1996; Scott et al., 1998; Luan and Burgos, 2010). Dissolved organic carbon (DOC) of the filtered solution was determined with an Analytik-jena multi N/C 2100 s series analyzer. Second, 0.5 mM uranyl acetate or 2 g/L NAu-2 was mixed with diluted rHA (100 ppm). The reduction extents of U(VI) and Fe(III) in NAu-2 were determined by measuring U(VI) and Fe(II) concentrations after 12 h of reaction (See section 2.7.1 below).

2.5. Experiments testing Fe(III)-HS/Fe(II)-HS complexes as electron shuttle to accelerate U(VI) and NAu-2 bioreduction

To test the electron shuttling role of Fe(III)-HS/Fe(II)-HS redox couple [from dissolution of clays and formation of Fe(III)/Fe(II)-HS complexes] to accelerate bioreduction of either U(VI) or Fe(III) in NAu-2, two separate experiments were conducted. First, oxygen-free ~ 400 µM of FeCl₂ and FeCl₃ were mixed with ~ 400 ppm HA for 24 h in BP buffer to obtain HA-Fe(II) and HA-Fe(III) complexes, respectively. Second, two separate experiments were conducted: (1) ~ 1.5 × 10⁸ cells/mL CN32 and 10 mM sodium lactate were added to HA-Fe(III) complex to test the ability of CN32 to reduce this complex. The final concentration of Fe³⁺ in HA-Fe(III) complex was ~ 200 µM. (2) Fe(II)-HA complex was added to either 0.5 mM uranyl acetate solution or 2 g/L NAu-2 suspension to test whether HA-complexed Fe²⁺ could abiotically reduce either U(VI) or structural Fe(III) in NAu-2. To test the possibility of mineral surface catalyzed U(VI) reduction by Fe(II)-HA complex, Fe-free kaolinite was added in some experiments. The final concentration of Fe²⁺ in HA-Fe(II) complex was ~ 200 µM.

For the two experiments, 0.4 mL samples were collected at the start point and after reaction for 4 h followed by centrifugation (10,000g, 10 min) and filtration (0.22 µm, nylon). Aqueous Fe²⁺ and Fe³⁺ concentrations of the filtrates were measured with the 1,10-phenanthroline method (see Section 2.7 for methods). Extra 0.1 mL samples were collected and mixed with 0.2 mL of 200 mM deoxygenated NaHCO₃ for 1 h to extract mineral-adsorbed U(VI) (Zhang et al., 2009). The mixtures were centrifuged (10,000g, 10 min) and filtered through a 0.22 µm nylon filter to collect the supernatant to measure aqueous U(VI) concentration by using the Arsenazo III method (see Section 2.7 for methods).

2.6. Adsorption of HA to clay minerals and characterization of residual aqueous HS

Humic acids were likely to adsorb to clay minerals (Wang and Xing, 2005; El-sayed et al., 2019), which may affect their roles in U(VI) reduction. Thus, adsorption experiments were performed by mixing 300 ppm HA with 2 g/L NAu-2 or SWy-2 in BP buffer.

The HA-clay suspensions were shaken on a horizontal shaker for 24 h to reach equilibrium (Ghosh et al., 2009). After centrifugation at 7,600g for 15 min, the supernatant was collected and stored in the dark at 4 °C for electron accepting capacity (EAC) and electron donating capacity (EDC) measurements (see Section 2.7 for methods).

2.7. Analytical methods

2.7.1. Measurements of concentrations of aqueous U(VI), total U, and Fe(II)

To monitor the progress of U(VI) and Fe(III) bioreduction, time course concentrations of aqueous U(VI) and total Fe(II) [including structural Fe(II) and aqueous Fe²⁺] were monitored. At selected time points, 0.2 mL sample was collected and mixed with 0.2 mL of 200 mM deoxygenated NaHCO₃ for 1 h to extract mineral-adsorbed U(VI) (Zhang et al., 2009). The mixture was centrifuged (10,000g, 10 min) and filtered through a 0.22 μm nylon filter to collect the supernatant. The supernatant was used to measure total U (VI) concentration [including aqueous and mineral-adsorbed U (VI)] according to the Arsenazo III spectrophotometric procedure (detection limit, 0.08 μM) (Sawin, 1961; Starvin and Rao, 2004). Briefly, 0.05 mL sample was mixed with 0.1 mL of 0.1 % Arsenazo III (0.1 g solid dissolved in 100 mL MQ-H₂O), 0.2 mL of 1 N HCl, and 0.65 mL MQ-H₂O to reach a total volume of 1 mL. The color was developed by placing the solution in the dark for 30 min and absorbance was measured at 655 nm using a UV-vis spectrophotometer (UV-2550, SHIMADZU). At the beginning and the end of the experiment, 0.2 mL sample was taken from the Balch bottles, centrifuged (10,000g, 10 min), filtered (0.22 μm, nylon), diluted with 2 % HNO₃ and re-filtered for total aqueous U concentration measurement with inductively coupled plasma optical emission spectroscopy (ICP-OES, Perkin Elmer, United States, detection limit, 0.08 μg/mL). The concentration of aqueous U(IV) was calculated by the difference in concentration between aqueous total U and U(VI).

To measure total Fe(II) concentration at selected time points, 0.6 mL suspension was collected from the Balch tubes with a syringe needle. Sample of 0.4 mL in volume was centrifuged (10,000 g, 10 min) and filtered (0.22 μm, nylon). The filtrate was used for aqueous Fe²⁺ measurement. The remaining 0.2 mL sample was used for total Fe(II) measurement. The concentrations of total Fe (II) and aqueous Fe²⁺ were measured using the 1,10-phenanthroline method (Amonette and Templeton, 1998). Briefly, 0.04 mL of 40 % HF, 0.48 mL of 1.8 N H₂SO₄ and 0.08 mL of 10 % freshly-prepared 1,10-phenanthroline (1 g reagent dissolved in 10 mL 95 % ethanol) were added to 0.2 mL samples followed by boiling to dissolve the structure of clay minerals [for total Fe(II)]. After the color development, absorbance at 510 nm was measured using a UV-vis spectrophotometer (UV-2550, SHIMADZU). Concentrations of total Fe and total aqueous Fe were determined using the same method after Fe(III) of clay suspension and aqueous Fe³⁺ were reduced to Fe(II) and Fe²⁺, respectively, with hydroxylamine hydrochloride. The extent of Fe(III) reduction was calculated based on the net amount of Fe(II) production at the end of reduction divided by the total Fe(III) concentration present in the starting minerals.

2.7.2. Reduction potential (E_h) measurement

To explain the thermodynamic favorability of redox reactions among HA, U(VI), and clay minerals, reduction potentials (E_h) of U(VI) and rHA were measured. Cyclic voltammetry experiments (Aeschbacher et al., 2011; Klüpfel et al., 2014) were conducted in 15 mL solutions with an electrochemical workstation (PGSTAT302N, Metrohm, Switzerland) using a glassy carbon disk working electrode, a platinum disk counter electrode, and an Ag/AgCl reference electrode (Yingchong Technology Inc., China). Cyclic

voltammograms (CVs) were obtained for 0.5 mM uranyl acetate in BP buffer and 100 ppm rHA. The CV scans were started at -1 V and ended at 0.9 V with 0.1 V/s scan rate and 0.001 sampling interval. After each series of CV experiments, the glassy carbon electrodes were replaced by a new one. For the measurement of rHA, 10 μM 1,1'-ethylene-2,2'-bipyridyldiylium dibromide (DQ, $E_h^0 = -0.35$ V) (Gorski et al., 2012) and 2,2'-azino-bis (3-ethylbenzothiazoline -6-sulphonic acid) (ABTS, $E_h^0 = +0.70$ V) (Gorski et al., 2012) were added to the solution to facilitate attainment of E_h equilibrium of rHA and electrodes (Aeschbacher et al., 2011). All the measurements were conducted in an anoxic glovebox at room temperature (N₂ atmosphere, O₂ < 0.1 ppm). The cathodic peak potentials (E_p^c) were the reduction potential (E_h) of the samples.

The E_h values of NAu-2 and SWy-2 were calculated using the following equation (Luan et al., 2014):

$$E_h = E_h^0 - 1/\beta \times 2.303 \times RT/nF \times \log[clay - Fe(II)]/[clay - Fe(III)]$$

where, E_h^0 is the standard state reduction potential of clay mineral, β is the fractional value, R is the universal gas constant, T is the absolute temperature (K), n is the stoichiometry of electron transfer between Fe(II) and Fe(III), F is the Faraday constant, [clay - Fe(II)] is the chemical activity of Fe(II) in clay mineral and [clay - Fe(III)] is the chemical activity of Fe(III) in clay mineral. For oxidized NAu-2 in this study, $E_h^0 = -0.34V$, $\beta = 0.36$, $n = 1$, [clay - Fe(II)] = $0.11 \times 10^{-3} mol/L$ and [clay - Fe(III)] = $7.73 \times 10^{-3} mol/L$; for oxidized SWy-2 in this study, $E_h^0 = -0.03V$, $\beta = 0.23$, $n = 1$, [clay - Fe(II)] = $0.08 \times 10^{-3} mol/L$ and [clay - Fe(III)] = $0.97 \times 10^{-3} mol/L$.

2.7.3. Electron accepting capacity (EAC) and electron donating capacity (EDC) measurements

Electron accepting capacity (EAC) and electron donating capacity (EDC) of HA stock and HA supernatants after adsorption to NAu-2 and SWy-2 (hereafter referred to as HA_{NAu-2} and HA_{SWy-2}, respectively) were measured to help explain various redox reactions between U(VI), Fe(II), HS, and microbes.

EAC and EDC measurements were conducted in an electrochemical cell filled with 10 mM of 80 mL deoxygenated PIPES buffer using an electrochemical workstation (PGSTAT302N, Metrohm, Switzerland), which was placed inside an anoxic glovebox at room temperature (N₂ atmosphere, O₂ < 0.1 ppm). Glassy carbon, coiled platinum wire auxiliary electrode, and Ag/AgCl electrode were selected as working electrode, counter electrode, and reference electrode, respectively. The potentials of the working electrode were equilibrated to $E_h = -0.49$ V in Mediated Electrochemical Reduction (MER) and $E_h = +0.61$ V in Mediated Electrochemical Oxidation (MEO) (Aeschbacher et al., 2010; Klüpfel et al., 2014). DQ and ABTS were chosen as electron transfer mediators for MER and MEO, respectively. After current was stabilized, 200 μL sample was injected to the cell. Quantitation of electrons transferred to and from samples was achieved by integration of MER and MEO current peaks. EAC and EDC values were calculated using the following equations (Klüpfel et al., 2014):

$$EAC = e_{accept}^- / m_{sample}. \quad (1)$$

$$EDC = e_{donate}^- / m_{sample}. \quad (2)$$

$$e_{accept}^- = \int I_{red} / Fdt. \quad (3)$$

$$e_{donate}^- = \int I_{ox} / Fdt. \quad (4)$$

$$m_{\text{sample}} = \text{DOC} * V_{\text{sample}} \quad (5)$$

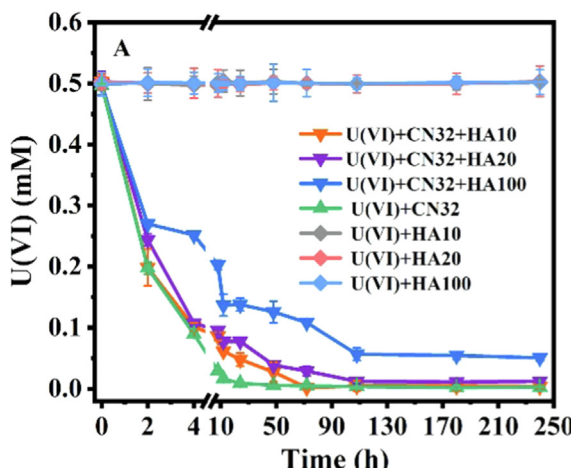
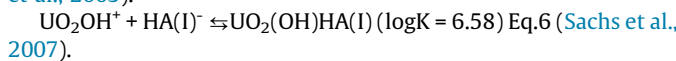
where e_{accept}^- and e_{donate}^- are the numbers of electrons transferred to and from samples, respectively. I_{red} and I_{oxy} are baseline-corrected reductive and oxidative currents in MER and MEO, respectively. Electrons transferred to/from samples were obtained by integrating the peak areas in current responses. V_{sample} is the volume of sample added to the electrochemical cell. The DOC of the supernatant was measured with an Analytik-jena multi N/C 2100 s series analyzer. $F (=96,485 \text{ sA/mol e}^-)$ is the Faraday constant.

2.7.4. Scanning electron microscope (SEM) observations

SEM and energy dispersive spectroscopy (EDS) were used to observe minerals and mineral-HS associations. At the start and the end of bioreduction, 20 μL suspension samples were drawn from the Balch bottles, deposited on poly-L-lysine covered glass coverslips, and allowed to settle for 15 min. The sample-coated coverslips were submerged in a fixative solution (2 % paraformaldehyde and 2 % glutaraldehyde in PBS buffer) for 30 min, followed by rinsing with PBS buffer three times. The PBS buffer consisted of 130 mM NaCl and 10 mM sodium phosphate. Afterwards, the fixed samples were sequentially dehydrated in 25 %, 50 %, 75 %, 95 % and 100 % ethanol solutions and followed by critical point drying (CPD). The coverslips were Pt-coated with a Quorum SC7620 Sputter Coater for SEM observations with a Zeiss Supra 55 SAPPHIRE scanning electron microscope (SEM) equipped with Genesis 2000 X-ray energy dispersive spectroscopy (EDS). An accelerating voltage of 10–15 kV and a working distance of 15 mm were used.

2.7.5. U(VI) speciation calculation

The thermodynamic stability and kinetic lability of U(VI) are controlled by its speciation, and the U(VI) speciation under the experimental conditions was calculated by using MINEQL (version 5.0). The reaction between U(VI) and HA to form complex of $\text{UO}_2(\text{-OH})(\text{HA})(\text{I})$ (Eq. 6) and the corresponding reaction constants were entered in MINEQL based on previous studies (Sachs et al., 2007; Tinnacher et al., 2013) where HA(I) denotes that one proton exchanging functional group of the HA participates in the reaction. All other aqueous reactions, including the formation of uranyl-carbonate species, were considered for the thermodynamic calculation with the database from a previous study (Guillaumont et al., 2003).



2.7.6. Kinetic analysis

Because of excess electron donor (lactate) in all treatments, the redox reaction rates were limited by electron acceptor. Thus, pseudo first order rate equations [$\ln(C) = -kt$] and [$\ln(C) = kt$] were used to describe U(VI) and Fe(III) bioreduction kinetics, respectively (Gu et al., 2005; Zeng et al., 2020a), where C was the concentration of either U(VI) or total Fe(II). The initial U(VI) reduction rate constants were calculated for the first 8 h because there was rapid decrease of U(VI) concentrations during this period. For the initial Fe(III) reduction rate constants, the first 4 h were chosen because Fe(II) concentrations increased rapidly during this period.

3. Results

3.1. U(VI) speciation

Based on thermodynamic calculations, $\text{UO}_2(\text{CO}_3)_2^{2-}$ (59 %) and $\text{UO}_2(\text{CO}_3)_3^{4-}$ (31 %) were the major U(VI) species in the presence of 30 mM of total CO_3^{2-} and 10 mM PIPES at neutral pH. Addition of 100 ppm HA did not alter the major U(VI) species at pH 7 based on the logK values reported for $\text{UO}_2(\text{OH})(\text{HA})$ from a previous study (Sachs et al., 2007) (Fig. S1).

3.2. Bioreduction of U(VI) in the presence of HS

The initial rate of U(VI) bioreduction was inhibited by the presence of HA, with a higher concentration of HA exhibiting a higher degree of inhibition (Fig. 1A, Table 1). The initial rate constants of U(VI) bioreduction decreased from $0.35 \pm 0.008 \text{ h}^{-1}$ for no-HA control to 0.21 ± 0.010 , 0.20 ± 0.002 , $0.10 \pm 0.001 \text{ h}^{-1}$ in the presence of 10, 20, and 100 ppm HA, respectively. Compared to HA, the effect of 20 ppm FA was negligible (Fig. 1B, Table 1). U(VI) was almost completely reduced after 240 h except in the 20 and 100 ppm HA experiments (Fig. 1, Table 1). In these two experiments, there were 0.01 and 0.05 mM U(VI) remaining at the end of the experiment (Table 2), likely because the reaction time was not long enough. Aqueous U(IV) was formed in the presence of 10, 20, and 100 ppm HA, and accounted for 2.00, 10.20 and 71.11 % of total U(IV), respectively (Table 2). To compare the effects of AQDS and HS on U(VI) bioreduction, additional experiments were performed in which HS was replaced by 0.1 mM (~40 ppm) AQDS. Results showed that AQDS increased the initial U(VI) bioreduction rate constant from $0.35 \pm 0.008 \text{ h}^{-1}$ to $0.43 \pm 0.018 \text{ h}^{-1}$ (Fig. 2), which was opposite to the effect of HS. HA or FA alone did not reduce

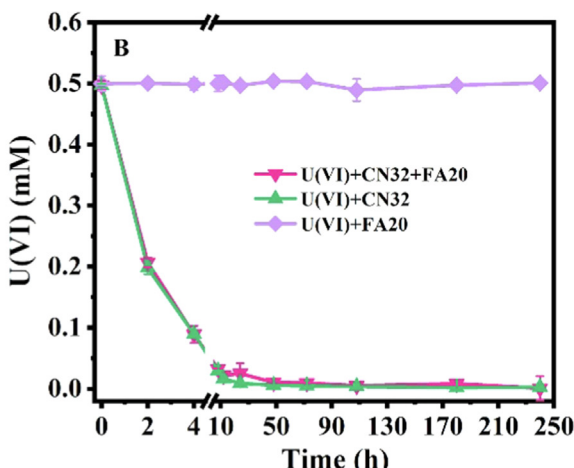


Fig. 1. Time-course decrease of U(VI) concentration during U(VI) reduction by *Shewanella putrefaciens* strain CN32 in BP buffer (pH 7). (A) in the presence of 10, 20, and 100 ppm HA; (B) in the presence of 20 ppm FA. The error bars represent one standard deviation from triplicate experiments.

Table 1

The initial rate constants (first 8 h) and the extents (by 240 h) of U(VI) reduction.

No.	Aim of experiment	Experimental Setup*	Reduction rate (h^{-1})	R^2	Reduction extent
1	Normal U(VI) bioreduction	U(VI) + CN32	0.35 ± 0.008	0.98	99.49 ± 0.21 %
2		U(VI) + CN32 + HA10	0.21 ± 0.010	0.80	99.26 ± 0.84 %
3		U(VI) + CN32 + HA20	0.20 ± 0.002	0.79	97.56 ± 0.46 %
4	Effect of HA/FA	U(VI) + CN32 + HA100	0.10 ± 0.001	0.77	89.77 ± 0.21 %
5		U(VI) + CN32 + FA20	0.34 ± 0.003	0.98	98.24 ± 1.42 %
6	Effect of AQDS	U(VI) + CN32 + AQDS	0.43 ± 0.018	0.97	99.43 ± 0.39 %
7	Effect of NAu-2	U(VI) + CN32 + NAu-2	0.05 ± 0.010	0.75	99.02 ± 0.15 %
8		U(VI) + CN32 + NAu-2 + HA10	0.09 ± 0.001	1.00	99.58 ± 0.72 %
9		U(VI) + CN32 + NAu-2 + HA20	0.11 ± 0.007	0.98	98.97 ± 0.10 %
10	Combined effect of HA/FA and NAu-2	U(VI) + CN32 + NAu-2 + HA100	0.12 ± 0.007	0.92	95.24 ± 0.36 %
11		U(VI) + CN32 + NAu-2 + FA20	0.09 ± 0.006	0.94	97.77 ± 0.24 %
12	Effect of AQDS in the presence of NAu-2	U(VI) + CN32 + NAu-2 + AQDS	0.32 ± 0.023	0.98	98.55 ± 0.13 %
13	Effect of SWy-2	U(VI) + CN32 + SWy-2	0.15 ± 0.030	0.97	99.31 ± 0.33 %
14		U(VI) + CN32 + SWy-2 + HA10	0.19 ± 0.008	0.98	95.37 ± 1.18 %
15		U(VI) + CN32 + SWy-2 + HA20	0.19 ± 0.006	0.99	94.26 ± 1.22 %
16	Combined effect of HA/FA and SWy-2	U(VI) + CN32 + SWy-2 + HA100	0.13 ± 0.001	0.83	93.13 ± 0.27 %
17		U(VI) + CN32 + SWy-2 + FA20	0.14 ± 0.005	0.97	98.47 ± 0.26 %

* U(VI): 0.5 mM uranyl acetate, CN32: 1.5×10^8 CFU/mL *Shewanella putrefaciens* CN32, HA10: 10 ppm humic acid, HA20: 20 ppm humic acid, HA100: 100 ppm humic acid, FA20: 20 ppm fulvic acid, AQDS: 0.1 mM anthraquinone-2,6-disulfonate, NAu-2: 2 g/L Fe-rich nontronite, and SWy-2: 2 g/L Fe-poor montmorillonite.

All experimental reactors contained 10 mM lactate as electron donor.

The sequence experimental numbers (No.) correspond to those in Table S1. The error bars represent one standard deviation of triplicate experiments (triplicate regressions).

Table 2

Aqueous U(VI) and U(IV) concentrations after 240 h.

No.	Experimental setups	U(VI) added at the start of reduction (mM)	U(VI) after reduction (mM)	Total U(IV) (mM)	Total aqueous U after reduction (mM)	Aqueous (IV)/Total U(IV)
1	U(VI) + CN32	0.50 ± 0	0 ± 0	0.50 ± 0	0 ± 0.01	0 ± 0
2	U(VI) + CN32 + HA10	0.50 ± 0.01	0 ± 0	0.50 ± 0.01	0.01 ± 0.02	2.00 ± 0.85 %
3	U(VI) + CN32 + HA20	0.50 ± 0.01	0.01 ± 0	0.49 ± 0.02	0.06 ± 0.04	10.20 ± 1.22 %
4	U(VI) + CN32 + HA100	0.50 ± 0.01	0.05 ± 0	0.45 ± 0.01	0.37 ± 0	71.11 ± 1.58 %
5	U(VI) + CN32 + FA20	0.50 ± 0.01	0.01 ± 0.01	0.49 ± 0	0 ± 0.01	0.17 ± 1.88 %
6	U(VI) + CN32 + NAu-2	0.49 ± 0.02	0 ± 0	0.49 ± 0.02	0.05 ± 0.02	0 ± 1.49 %
7	U(VI) + CN32 + NAu-2 + HA10	0.50 ± 0.01	0.01 ± 0	0.49 ± 0.01	0.01 ± 0.01	0 ± 1.12 %
8	U(VI) + CN32 + NAu-2 + HA20	0.49 ± 0.01	0 ± 0	0.49 ± 0.01	0 ± 0.01	0 ± 1.04 %
9	U(VI) + CN32 + NAu-2 + HA100	0.48 ± 0.02	0.02 ± 0	0.46 ± 0.02	0.02 ± 0.01	0 ± 2.88 %
10	U(VI) + CN32 + NAu-2 + FA20	0.50 ± 0.02	0.01 ± 0	0.49 ± 0.02	0.01 ± 0.01	0 ± 1.50 %
11	U(VI) + CN32 + SWy-2	0.50 ± 0	0 ± 0	0.50 ± 0.01	0.03 ± 0.01	0 ± 1.61 %
12	U(VI) + CN32 + SWy-2 + HA10	0.50 ± 0.03	0.02 ± 0.01	0.48 ± 0.02	0.02 ± 0.02	0 ± 0.73 %
13	U(VI) + CN32 + SWy-2 + HA20	0.49 ± 0.01	0.03 ± 0.01	0.46 ± 0	0.03 ± 0.01	0 ± 1.48 %
14	U(VI) + CN32 + SWy-2 + HA100	0.50 ± 0.02	0.03 ± 0	0.47 ± 0.02	0.20 ± 0.01	36.17 ± 0.86 %
15	U(VI) + CN32 + SWy-2 + FA20	0.50 ± 0.01	0.01 ± 0	0.49 ± 0.01	0.01 ± 0.01	0 ± 2.35 %

U(VI) concentration was measured with the Arsenazo III spectrophotometric procedure (Sawin, 1961; Starvin and Rao, 2004) with UV-vis spectrophotometer (UV-2550, SHIMADZU).

Total aqueous U concentration was measured with inductively coupled plasma optical emission spectroscopy (ICP-OES, Perkin Elmer, United States).

The error bars represent one standard deviation of triplicate experiments.

U(VI) at neutral pH (Fig. 1), consistent with previous studies (Nash et al., 1984; Gu and Chen, 2003).

3.3. Bioreduction of Fe(III)-bearing clay minerals in the presence of HS

Relative to no-HA control, the initial rate of Fe(III) bioreduction in NAu-2 increased by a factor of 5 in the presence of HA. The extent also increased from 24.39 % to 32.12 %, 32.71 %, and 37.44 % in the presence of 10, 20 and 100 ppm HA, respectively (Fig. 3A-C, Table S2). In addition to the role of HA serving as electron shuttle directly (Liu et al., 2017), another possibility was that HA dissolved some NAu-2 during bioreduction, and the released aqueous Fe^{3+} and Fe^{2+} complexed with HA to form HA-Fe(III)/HA-Fe(II) complexes. These complexes may have served as an electron shuttle as well. Indeed, both aqueous Fe^{2+} and Fe^{3+} were measured in these ternary systems (Table S3). To test this mechanism, additional control experiments were conducted. Results showed that, within 4 h, CN32 cells reduced 89 %

Fe(III)-HA complex to Fe(II)-HA complex (Fig. S2A). The resulting Fe(II)-HA complex reduced 33 % structural Fe(III) in NAu-2 (Fig. S2B), suggesting that Fe(III)-HA/Fe(II)-HA complexes indeed served as an electron shuttle to enhance Fe(III) bioreduction. For Fe-poor SWy-2, HA only slightly enhanced the rate of Fe(III) bioreduction (Fig. 4A-C, Table S2), but not the extent. Compared to HA, the enhancement effect of FA was weaker for both NAu-2 and SWy-2 (Fig. 3D and 4D, Table S2). Abiotic reduction of Fe(III) in these two clay minerals by original (oxidized) HA or FA was negligible (Figs. 3 and 4).

3.4. Bioreduction of U(VI) in the presence of clay minerals

Both NAu-2 and SWy-2 greatly inhibited the rate of U(VI) bioreduction (Fig. 5A, Table 1). In the presence of NAu-2, there was a “lag phase” of U(VI) reduction in the first 4 h (Fig. 5A), suggesting that the initial U(VI) reduction rate (rate constat ≈ 0) was greatly inhibited. In the presence of SWy-2, U(VI) bioreduction did not

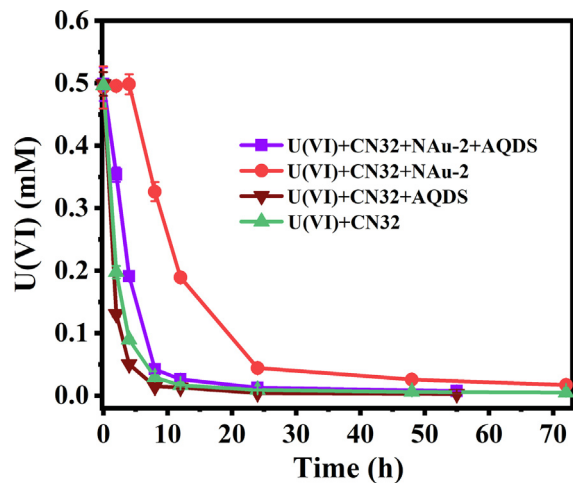


Fig. 2. Time-course decrease of U(VI) concentration during U(VI) reduction by *Shewanella putrefaciens* strain CN32 in the presence of AQDS in BP buffer (pH 7). The error bars represent one standard deviation from triplicate experiments.

show a “lag phase” (Fig. 5A), but the initial reduction rate decreased (rate constant decreased from $0.35 \pm 0.008 \text{ h}^{-1}$ to $0.15 \pm 0.030 \text{ h}^{-1}$). The final reduction extent of U(VI) was not affected by either NAu-2 or SWy-2. At the end of reaction, U(VI) concentration was below detection limit ($0.08 \mu\text{M}$) in all treatments (Fig. 5A)

and no aqueous U(IV) was detected (Table 2), suggesting uraninite precipitation, which was consistent with our previous study (Zhang et al., 2021).

3.5. Bioreduction of Fe(III) in clay minerals in the presence of U(VI)

The initial reduction rate and the final reduction extent of structural Fe(III) in NAu-2 were enhanced in the presence of U(VI) (Fig. 5B, Table S2). Compared to no-U(VI) control, the initial reduction rate constant and reduction extent of Fe(III) in NAu-2 increased from $0.10 \pm 0.019 \text{ h}^{-1}$ and $24.39 \pm 0.31 \%$ to $0.68 \pm 0.016 \text{ h}^{-1}$ and $37.41 \pm 0.46 \%$, respectively, in the presence of 0.5 mM U(VI). The presence of U(VI) also increased the bioreduction rate constant of structural Fe(III) in SWy-2 from $0.21 \pm 0.013 \text{ h}^{-1}$ to $0.38 \pm 0.009 \text{ h}^{-1}$, however, this enhancement effect was much smaller than that of NAu-2 (Fig. 5B, Table S2). In these systems [U + CN32 + NAu-2/SWy-2], aqueous Fe²⁺ and Fe³⁺ were very low (Table S3).

3.6. Bioreduction of U(VI) in the presence of both HS and clay minerals

Although HS and clay minerals both inhibited U(VI) bioreduction (Figs. 1 and 5A), the effect of their combination was not a simple addition of the two inhibitory effects, likely due to the complex reaction among HS, clay minerals and U(VI).

Relative to NAu-2 alone, addition of HS partially alleviated its inhibitory effect on U(VI) bioreduction (Fig. 6). Furthermore, the

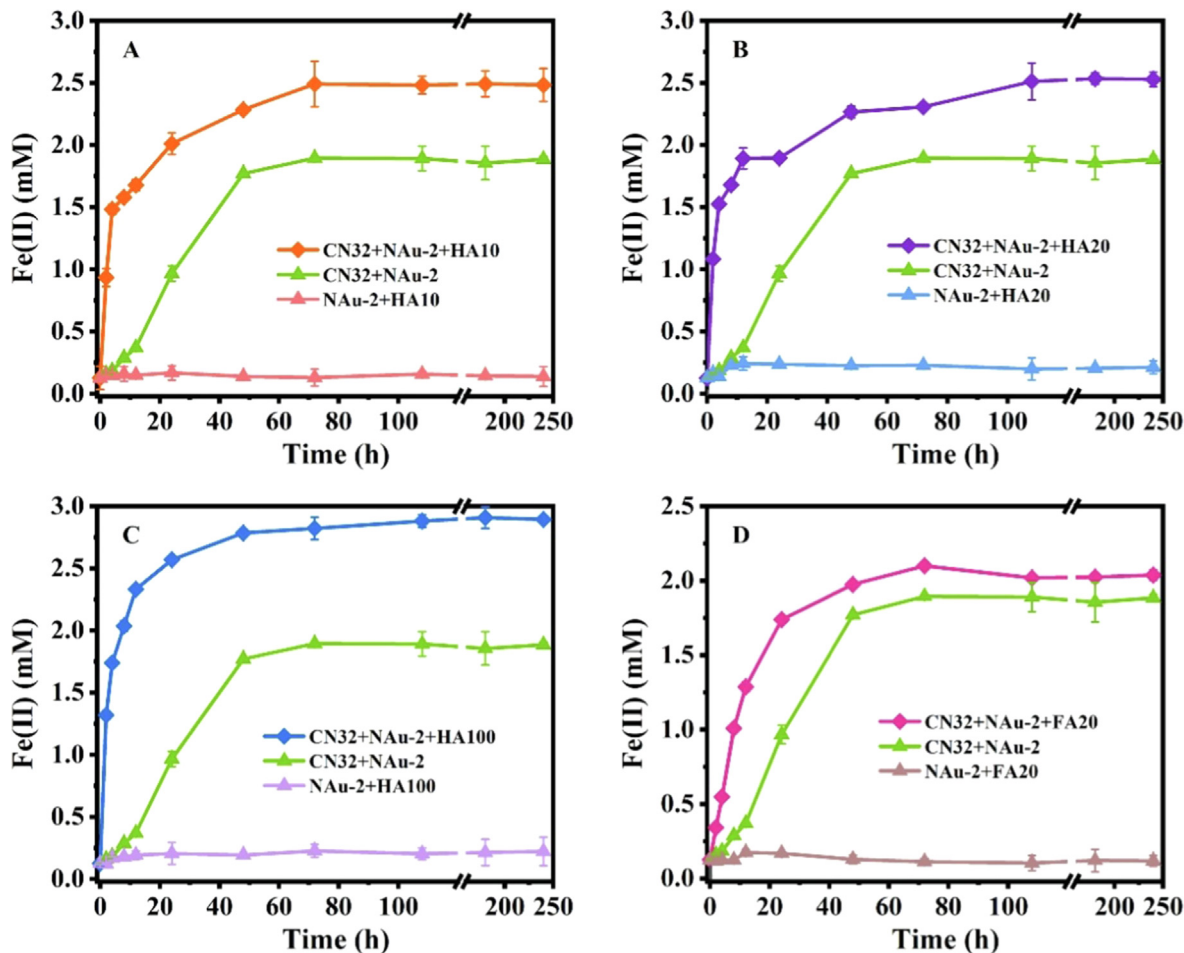


Fig. 3. Time-course increase of Fe(II) concentration during reduction of structural Fe(III) in nontronite NAu-2 by *Shewanella putrefaciens* strain CN32 in the presence of 10 ppm HA (A), 20 ppm HA (B), 100 ppm HA (C) and 20 ppm FA (D) in BP buffer (pH 7). The error bars represent one standard deviation of triplicate experiments.

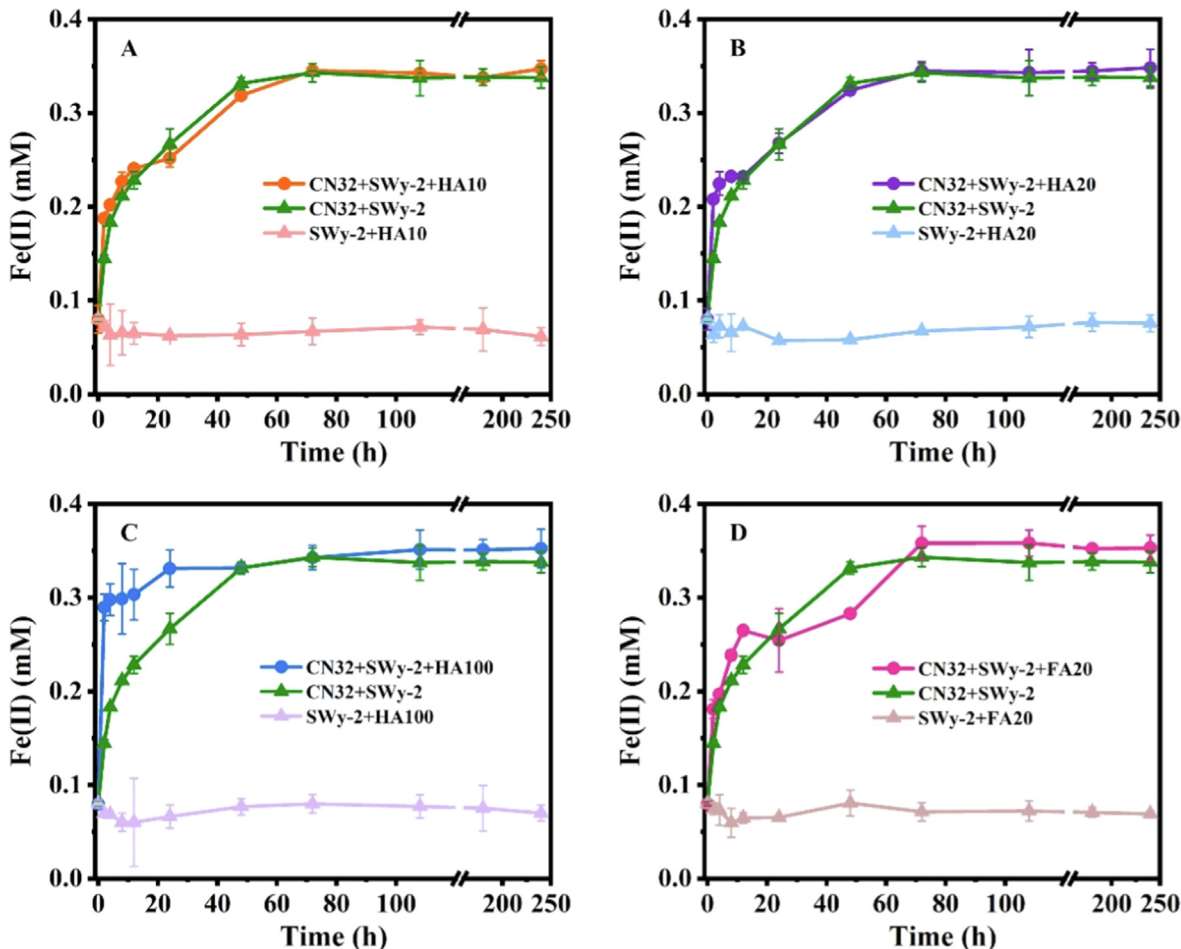


Fig. 4. Time-course increase of Fe(II) concentration during reduction of structural Fe(III) in montmorillonite SWy2 by *Shewanella putrefaciens* strain CN32 in the presence of 10 ppm HA (A), 20 ppm HA (B), 100 ppm HA (C) and 20 ppm FA (D) in BP buffer (pH 7). The error bars represent one standard deviation of triplicate experiments.

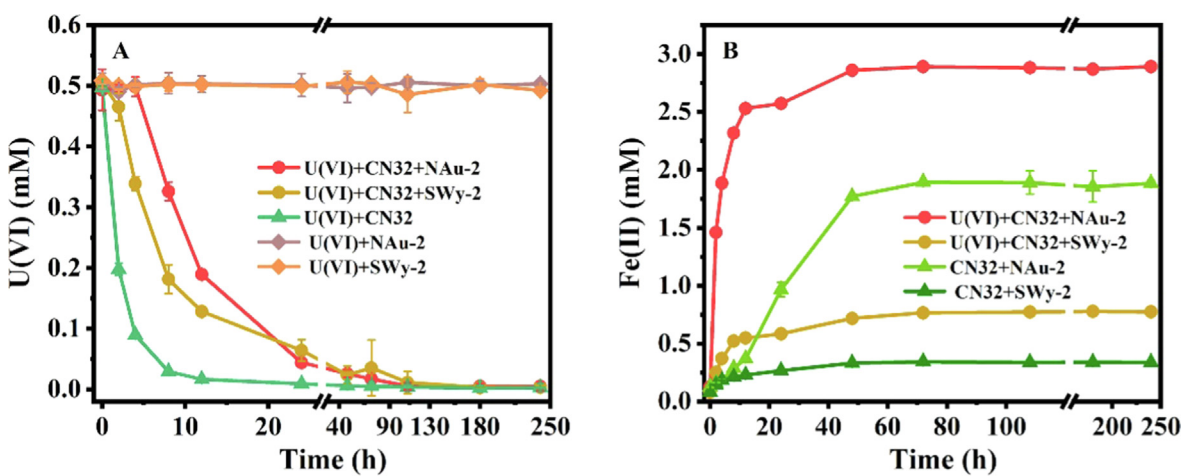


Fig. 5. U(VI) bioreduction in the presence of NAu-2 or SWy-2 in BP buffer (pH 7). (A) Time-course decrease of U(VI) concentration. (B) Time-course increase of total Fe(II) in NAu-2 or SWy-2. The error bars represent one standard deviation of triplicate experiments.

“lag phase” observed in the ternary system (Fig. 5A) disappeared. More quantitatively, addition of 10, 20, 100 ppm HA and 20 ppm FA increased the U(VI) bioreduction rate constants from $0.05 \pm 0.010 \text{ h}^{-1}$ to 0.09 ± 0.001 , 0.11 ± 0.007 , 0.12 ± 0.007 , $0.09 \pm 0.006 \text{ h}^{-1}$, respectively (Table 1). To determine if the aqueous HA-Fe(III)/

HA-Fe(II) complexes served as an electron shuttle to enhance U(VI) bioreduction, a control experiment was conducted, similar to that for Fe(III) bioreduction (Section 3.3). Results showed that Fe(II)-HA complex did not reduce U(VI), even in the presence of kaolinite surface (Fig. S2C), suggesting that the redox couple of

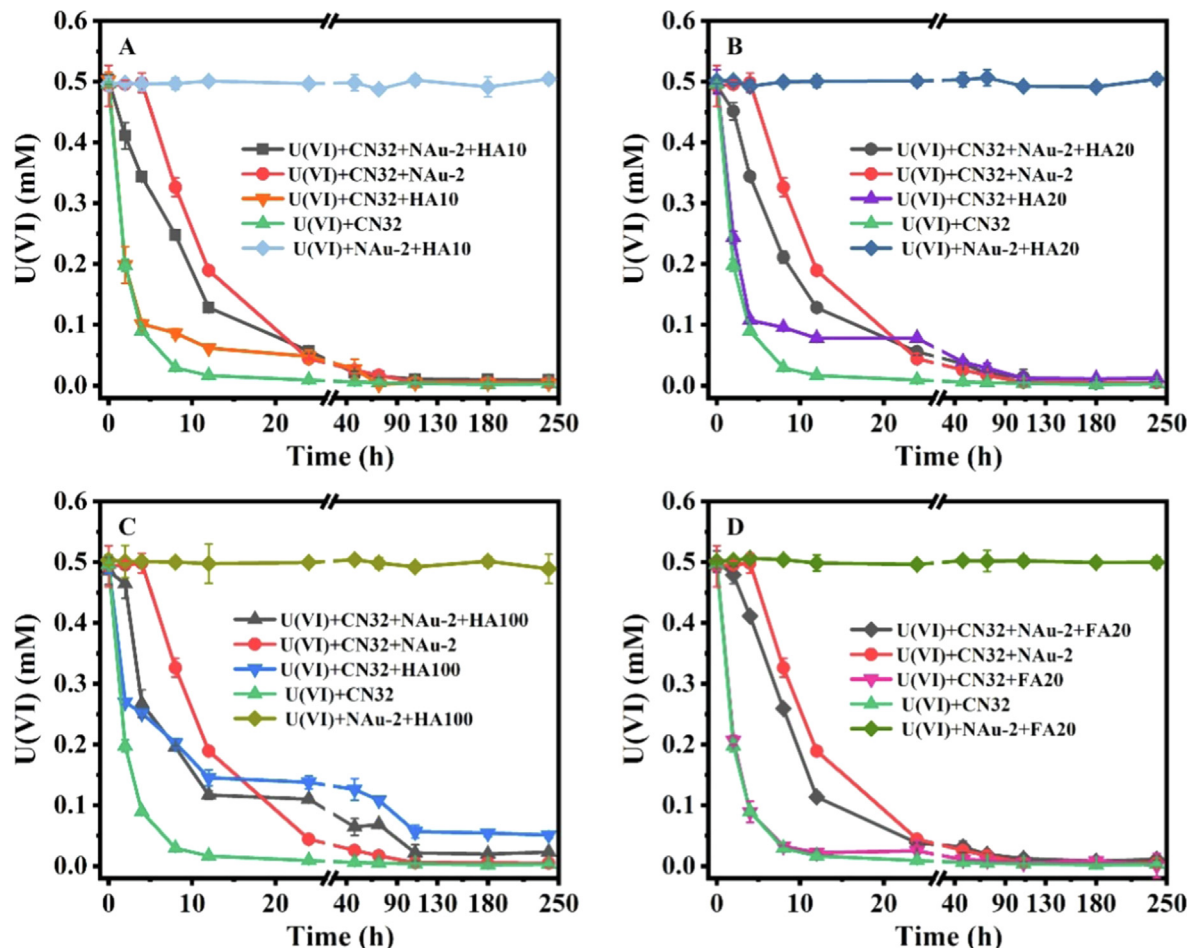


Fig. 6. Time-course decrease of U(VI) concentration during U(VI) reduction by *Shewanella putrefaciens* strain CN32 in the presence of both nontronite (NAu-2) and 10 ppm HA (A), 20 ppm HA (B), 100 ppm HA (C) and 20 ppm FA (D) in BP buffer (pH 7). The error bars represent one standard deviation from triplicate experiments.

Fe(III)-HA/Fe(II)-HA complexes did not serve as an electron shuttle to enhance U(VI) bioreduction, which was different from its role in Fe(III) bioreduction. Therefore, the role of HS in partially alleviating the inhibitory effect of clay minerals on U(VI) bioreduction may be due to other reasons [i.e., less electron diversion to clay minerals due to accelerated Fe(III) reduction by HS, see Section 3.7]. Addition of HS to SWy-2 experiments also enhanced the initial rate of U(VI) bioreduction, with HA showing a greater effect than FA (Fig. 7, Table 1). Compared to HS, addition of its analogue AQDS exhibited a greater stimulation on the rate of U(VI) bioreduction (up to $0.32 \pm 0.023 \text{ h}^{-1}$) (Fig. 2, Table 1).

Compared to HS alone, addition of clay minerals to the ternary systems of U(VI) + CN32 + HS further inhibited the initial bioreduction rate of U(VI), with NAu-2 having a greater inhibitory effect than SWy-2 (Figs. 6 and 7, Table 1), similar to that observed in the ternary system [U(VI) + CN32 + clay]. However, there was one complication for the quaternary system [U(VI) + CN32 + HS + clay] at 100 ppm HA. As expected, addition of NAu-2 further inhibited U(VI) bioreduction rate in the first 4 h. However, subsequently (4–12 h), the presence of NAu-2 partially negated the inhibitory effect of HS (Fig. 6C). This time-dependent effect was more obvious in the presence of SWy-2, where addition of SWy-2 inhibited U(VI) bioreduction within the first 2 h, but subsequently negated the inhibitory effect of 100 ppm HA (Fig. 7C). In contrast, such time-dependent effect was absent in the case of AQDS, and addition of NAu-2 inhibited the U(VI) bioreduction rate throughout the entire time period (Fig. 2, Table 1).

In the presence of both HS and clay minerals, bioreduced U(IV) was mostly sequestered in the solid, with the exception of the combination of SWy-2 and 100 ppm HA (Table 2). SEM images showed that at the start of reaction, the surfaces of NAu-2 and SWy-2 were covered by C-rich materials, and no obvious U signal was found (Fig. S3). However, by the end of bioreduction, the surfaces of NAu-2 and SWy-2 were covered by C-rich and U-rich materials (Fig. 8). Relative to the ternary system of U(VI) + CN32 + HA with 2.00 %, 10.20 % and 71.11 % aqueous U(IV) at 10, 20, and 100 ppm HA, respectively, addition of NAu-2 sequestered all U(IV) into solid (Table 2). However, addition of SWy-2 to the U + CN32 + HA100 system did not completely sequester U(IV) into the solid, and there was 36.17 % remaining in solution (Table 2). Similar to the ternary systems [CN32 + U(VI) + FA], U(IV) also remained in the solid after addition of NAu-2 or SWy-2 to the U(VI) + CN32 + FA (20 ppm) system (Table 2).

3.7. Bioreduction of Fe(III) in clay minerals in the presence of both HS and U(VI)

To help explain the U(VI) bioreduction kinetics in the presence of both HS and clay minerals, it was important to understand Fe(III) bioreduction kinetics in the same systems. In this case, HS and U(VI) individually enhanced Fe(III) bioreduction, and the effect of their combination was stronger than either one, which was different from the combined effect of HS and clay minerals on U(VI) bioreduction.

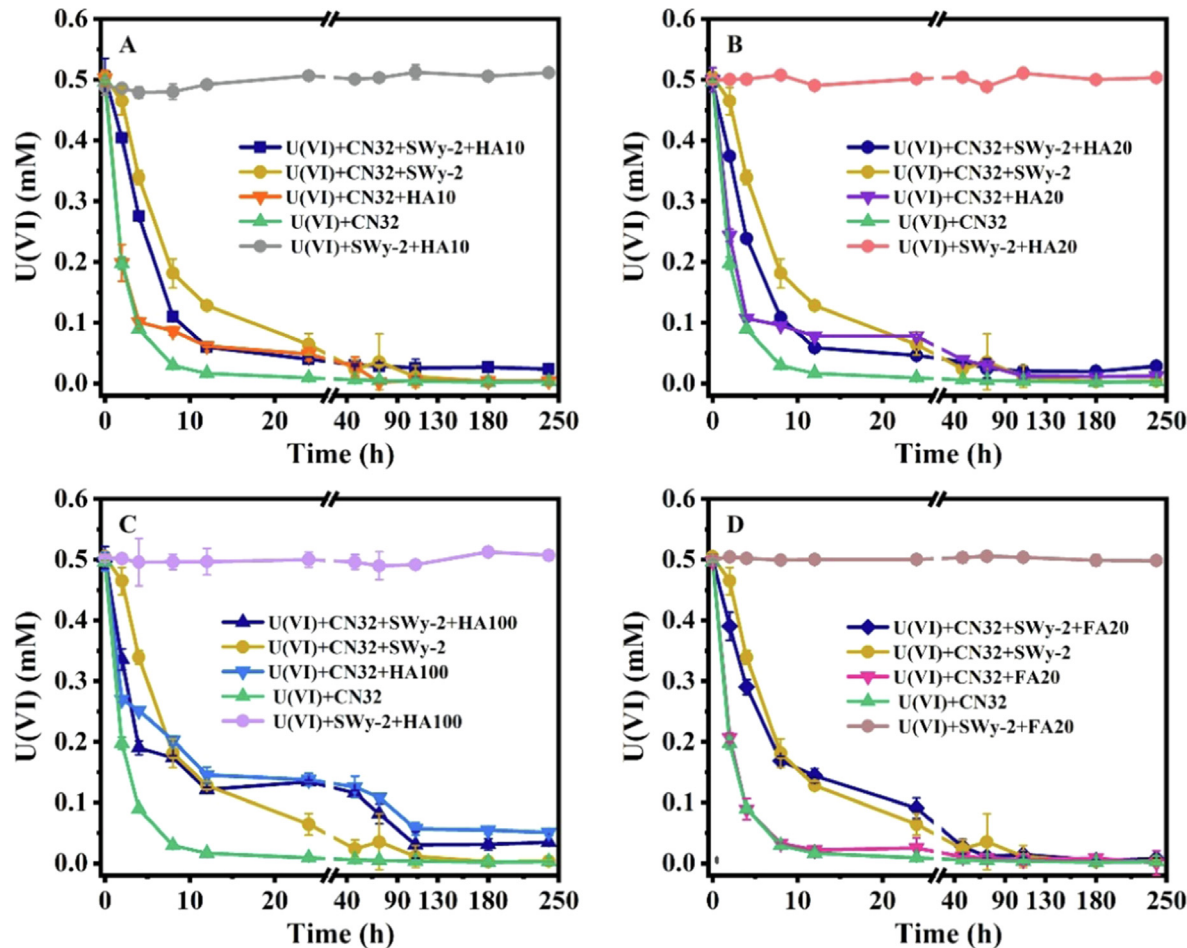


Fig. 7. Time-course decrease of U(VI) concentration during U(VI) reduction by *Shewanella putrefaciens* strain CN32 in the presence of both montmorillonite (SWy-2) and 10 ppm HA (A), 20 ppm HA (B), 100 ppm HA (C) and 20 ppm FA (D) in BP buffer (pH 7). The error bars represent one standard deviation of triplicate experiments.

Compared to U(VI) only, addition of HA increased the initial reduction rate of Fe(III) in both NAu-2 and SWy-2, with a higher HA concentration showing a greater effect (Fig. 9A-C, and 10A-C, Table S2). HA showed a greater effect than FA at the same concentration (Fig. 9B, 9D, 10B and 10D, Table S2). Addition of HA also increased the extent of Fe(III) reduction in NAu-2, but not in SWy-2 (Fig. 9A-C and 10A-C, Table S2), similar to its effect in the ternary systems (Fig. 3A-C and 4A-C). Compared to HS alone, addition of U(VI) enhanced both the initial rate and extent of Fe(III) bioreduction in NAu-2 and SWy-2 (Figs. 9 and 10, Table S2), similar to the effect of U(VI) in the ternary systems [U(VI) + CN32 + clay] (Fig. 5B, Table S2).

3.8. Adsorption of U(VI) to clay minerals

U(VI) adsorption experiments showed that under the experimental conditions of this study (i.e., in 30 mM NaHCO₃ and 10 mM PIPES buffer), there were only 4.12 % and 5.41 % U(VI) adsorption to NAu-2 and SWy-2, respectively (Fig. S4). Addition of 100 ppm HA and extension of reaction time did not increase the amount of U(VI) adsorption (Fig. S4).

3.9. Abiotic reduction of U(VI) and NAu-2 by bioreduced HA

Bioreduction results demonstrated that HA inhibited the bioreduction of U(VI) (Fig. 1), which was in direct contrast to its enhancement effect on the Fe(III) bioreduction (Fig. 3A-C and 4A-C). This may be due to the difference in reduction potential (E_h) between U(VI) and oxidized clay minerals. To confirm this,

E_h values of U(VI) and CN32-reduced HA (rHA) were measured under experimental conditions and E_h values of oxidized clay minerals were calculated based on a previous study (Luan et al., 2014). Results showed that rHA (-0.044 V) had a higher (less negative) E_h than that of U(VI) (-0.126 V) (Fig. S5, Table 3), suggesting that electron transfer from rHA to un-complexed U(VI) was not favorable. In our experimental system at neutral pH, U(VI) did not complex with HA (Fig. S1). In contrast, rHA had a lower reduction potential than oxidized NAu-2/SWy-2 (-0.037 V and + 0.248 V, respectively), suggesting that electron transfer from rHA to structural Fe(III) in these clays was favorable, which was further confirmed by abiotic reduction experiments. After 12 h reaction, about 0.15 mM Fe(III) in NAu-2 was reduced by rHA. However, U(VI) was not reduced by rHA within the same time period.

3.10. Adsorption of HA to clay minerals

Previous studies showed that HA may adsorb onto the surface of clay minerals (Wang and Xing, 2005; Zhang et al., 2012; Liu et al., 2017), and the EDC and EAC of the residual aqueous fraction may be different from those of bulk HA, which may change the properties of HA and its effect on U(VI) bioreduction. This selective adsorption of HA may explain the time-dependent effect of HA and clay minerals on U(VI) bioreduction in the quaternary systems (Fig. 6C and 7C). Therefore, EDC and EAC values of bulk HA and residual aqueous fractions after adsorption to NAu-2 and SWy-2 were measured (Fig. S6). Before adsorption to clay minerals, the EDC [1.11 mmol e⁻/(g HA)] of bulk HA was lower than the EAC

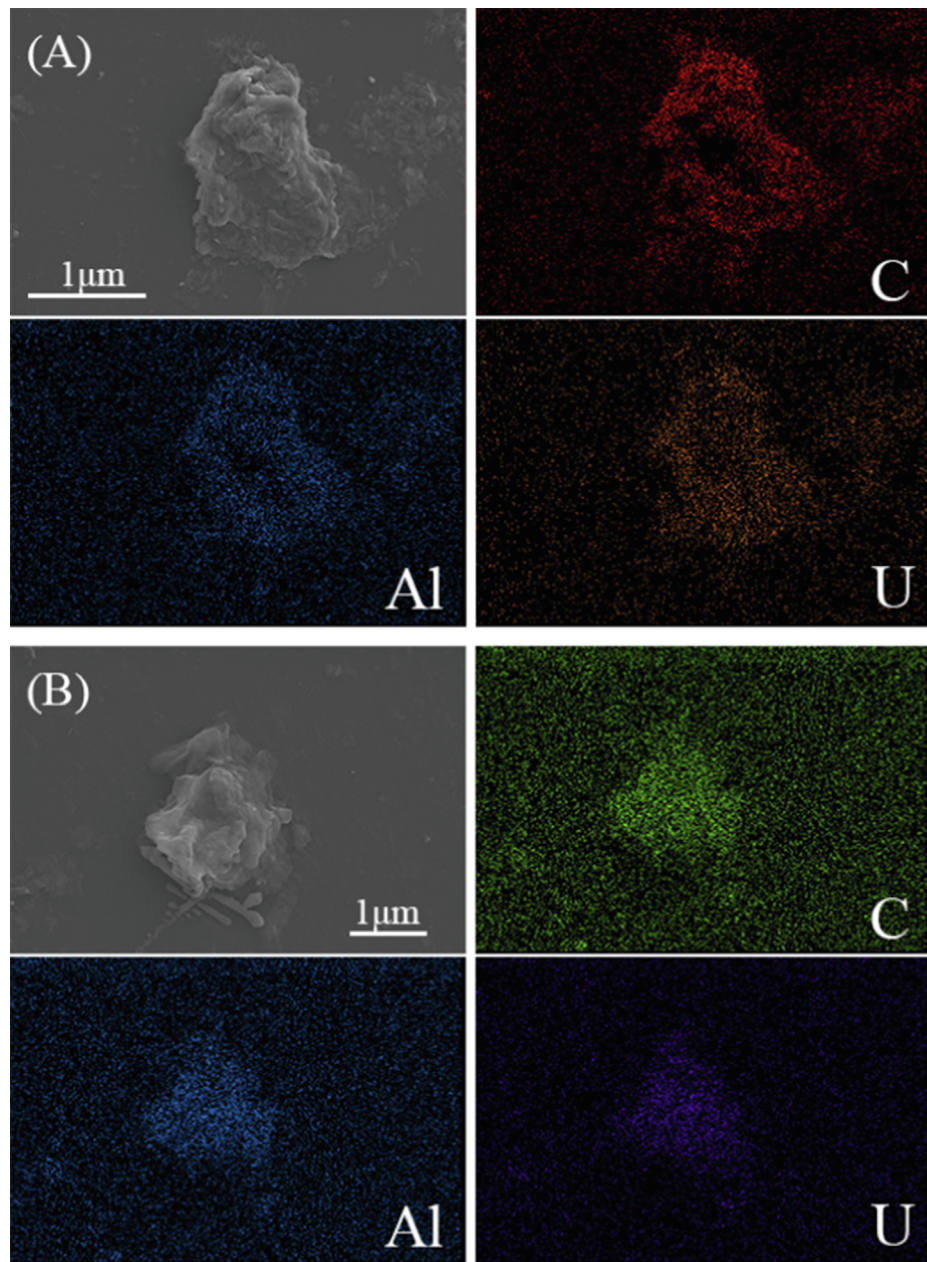


Fig. 8. (A) SEM image of nontronite NAu-2 and elemental maps of C, U and Al after reduction by *Shewanella putrefaciens* strain CN32 in the presence of U(VI) and 100 ppm HA. (B) SEM image of montmorillonite SWy-2 and elemental maps of C, U and Al after reduction by *Shewanella putrefaciens* strain CN32 in the presence of U(VI) and 100 ppm HA.

[3.13 mmol e⁻/(g HA)]. After adsorption to NAu-2 and SWy-2, the EDC of the residual aqueous fractions increased to 2.00 and 1.93 mmol e⁻/(g HA), respectively, and the EAC values decreased to 0.31 and 0.39 mmol e⁻/(g HA), respectively. The EDC values of the residual aqueous fractions after adsorption of HA to clay minerals were higher than EAC values, which was opposite to those of bulk HA. Therefore, selective adsorption of HA to clay surface may have accounted for its decreased ability to retain electrons and thus partially negated the inhibitory effect of HA.

4. Discussion

4.1. the effect of HS on the bioreduction of U(VI)

Under anoxic condition, HS may accept electrons from microbial respiration and be reduced (Lovley et al., 1996; Klüpfel et al.,

2014). Therefore, HS may compete with other terminal electron acceptors such as SO₄²⁻ and CO₂ to inhibit their bioreduction (Heitmann et al., 2007; Klüpfel et al., 2014). In the present study, HA showed an inhibitory effect on U(VI) bioreduction (Fig. 1A, Table 1), which was likely because HA competed against U(VI) for electrons from CN32. HA had a high EAC of 3.13 mmol e⁻/(g HA), however, reduced HA (rHA) did not reduce U(VI). Therefore, HA accepted electrons from CN32 but did not donate them to U(VI) (Fig. 11A), due to the higher E_h of rHA than that of U(VI) (Table 3), which would inhibit the initial rate of U(VI) bioreduction. However, a previous study (Gu et al., 2005) showed an enhancement effect of soil HA on U(VI) bioreduction. A likely reason for this discrepancy was different types of HA used. HA from different sources may possess different aromaticity and E_h values, with more aromatic HA possessing lower E_h values (Aeschbacher et al., 2011). A previous study showed that soil HA was more aromatic than peat HA (Aristilde and Sposito, 2013). Thus, the E_h value of

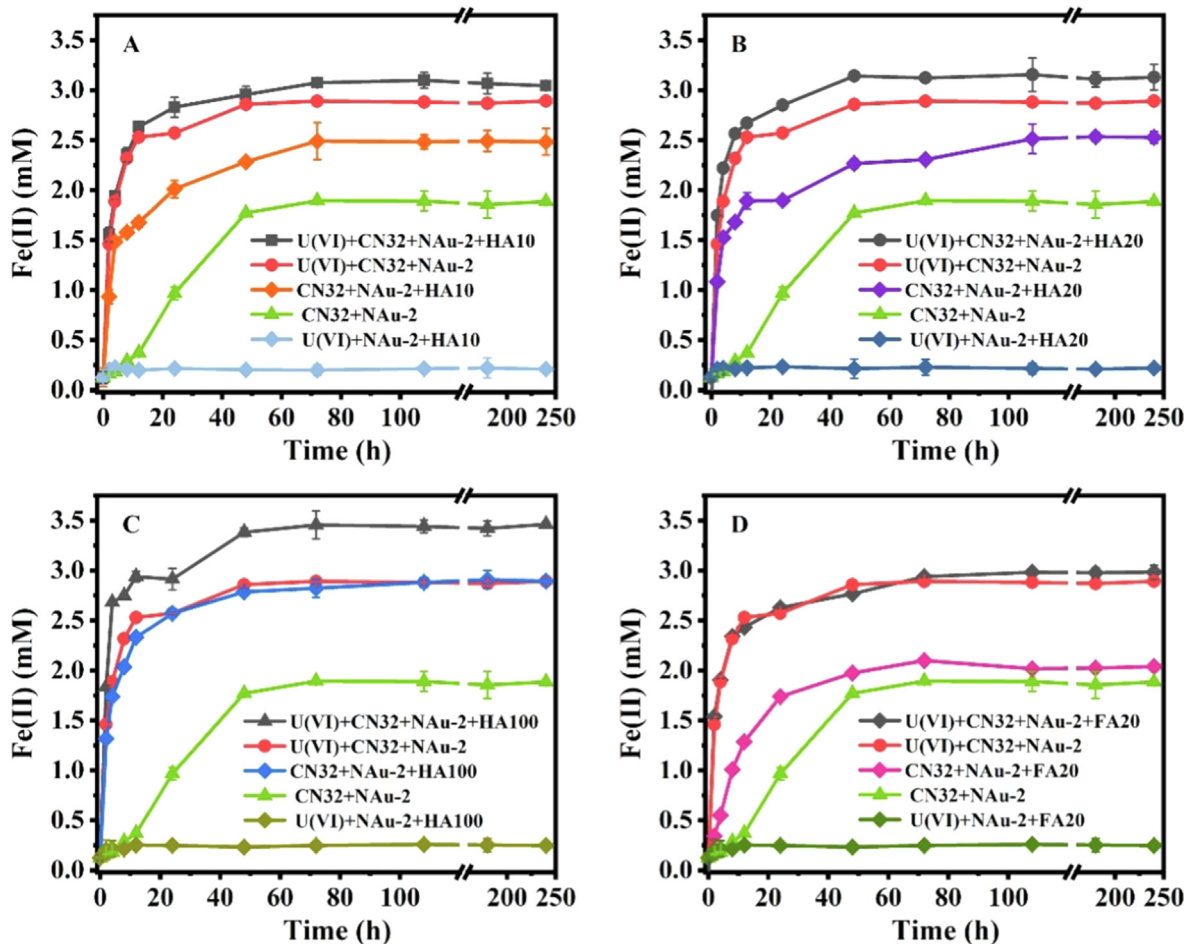


Fig. 9. Time-course increase of Fe(II) concentration in nontronite (NAu-2) during U(VI) bioreduction in the presence of both nontronite (NAu-2) and 10 ppm HA (A), 20 ppm HA (B), 100 ppm HA (C) and 20 ppm FA (D) in BP buffer (pH 7). The error bars represent one standard deviation of triplicate experiments.

reduced soil HA used in the Gu et al. study might be lower than that of reduced peat HA used in this study, which would make it possible to transfer electrons from reduced soil HA to U(VI), but not from reduced peat HA to U(VI). Therefore, soil HA could serve as an electron shuttle between CN32 and U(VI) to accelerate the bioreduction of U(VI) (Gu et al., 2005), but peat HA may not have this function. Additionally, a slight difference in experimental pH (7.5 in the Gu et al. study versus 7 in this study) may be another reason for the different effect of HS on U(VI) reduction, because of pH-dependent U(VI) speciation (Fig. S1).

Compared to HA, FA showed a negligible effect on the bioreduction of U(VI) (Fig. 1, Table 1), likely because FA has a smaller molecular size and a less amount of poly-condensed aromatic structures (Scott et al., 1998; Chen et al., 2003; Gu and Chen, 2003), which are considered to be the main electron accepting moieties in HS (Scott et al., 1998). Indeed, FA has a lower EAC than HA (Scott et al., 1998; Aeschbacher et al., 2010), therefore it should have received and possibly retained fewer electrons from CN32.

A previous study showed that U(VI) could complex with HS to form U(VI)-HS complex in the absence of (bi)carbonates (Sachs et al., 2007), which may influence U(VI) bioreduction kinetics. However, based on thermodynamic calculations, the major U(VI) species were $\text{UO}_2(\text{CO}_3)_2^{2-}$ and $\text{UO}_2(\text{CO}_3)_3^{4-}$ in the presence of 100 ppm HA and 30 mM bicarbonate (Fig. S1). The difference in the dominant U(VI) species between our study and Sachs et al. was mainly due to the presence of 30 mM bicarbonate in our study. A previous study also showed that U(VI)-HA/U(VI)-FA complexes

were not the dominant species when the system was in equilibrium with the atmosphere and 10 ppm HA/FA (Lenhart, 1998). Some studies have used (bi)carbonates to extract U(VI) in soils (Zhou and Gu, 2005; Choy et al., 2006), because U(VI) forms more stable complexes with carbonates than HA/FA. Therefore, U(VI)-HA/U(VI)-FA complex formation was not expected to be the key factor that affected U(VI) bioreduction kinetics under our experimental conditions.

AQDS, which contains similar redox-active functional groups (such as quinones), is commonly used as an HS analogue to accelerate the bioreduction rates of oxidized metals such as Fe (III), Cr(VI) and U(VI) by serving as an electron shuttle (Dong et al., 2009; Zhang et al., 2009; Meng et al., 2018). However, the inhibitory effect of HA on U(VI) bioreduction (Fig. 1A) observed in this study was in contrast to the stimulatory effect of AQDS (Fig. 2), suggesting that AQDS does not fully represent the role of HS in the environment when it comes to U(VI) bioreduction.

4.2. the effect of HS on the bioreduction of Fe(III) in clay minerals

In contrast to U(VI), the Fe(III) bioreduction rate and extent in NAu-2 were enhanced in the presence of HA and FA (Fig. 3, Table S2). There were two possible mechanisms to explain this enhancement effect. One possibility was that HA directly acted as an electron shuttle between Fe(III) and microbes (Scott et al., 1998; Liu et al., 2017; Yu et al., 2021) (Fig. 11B), which is similar to AQDS (Dong et al., 2009). Indeed, rHA had a lower reduction

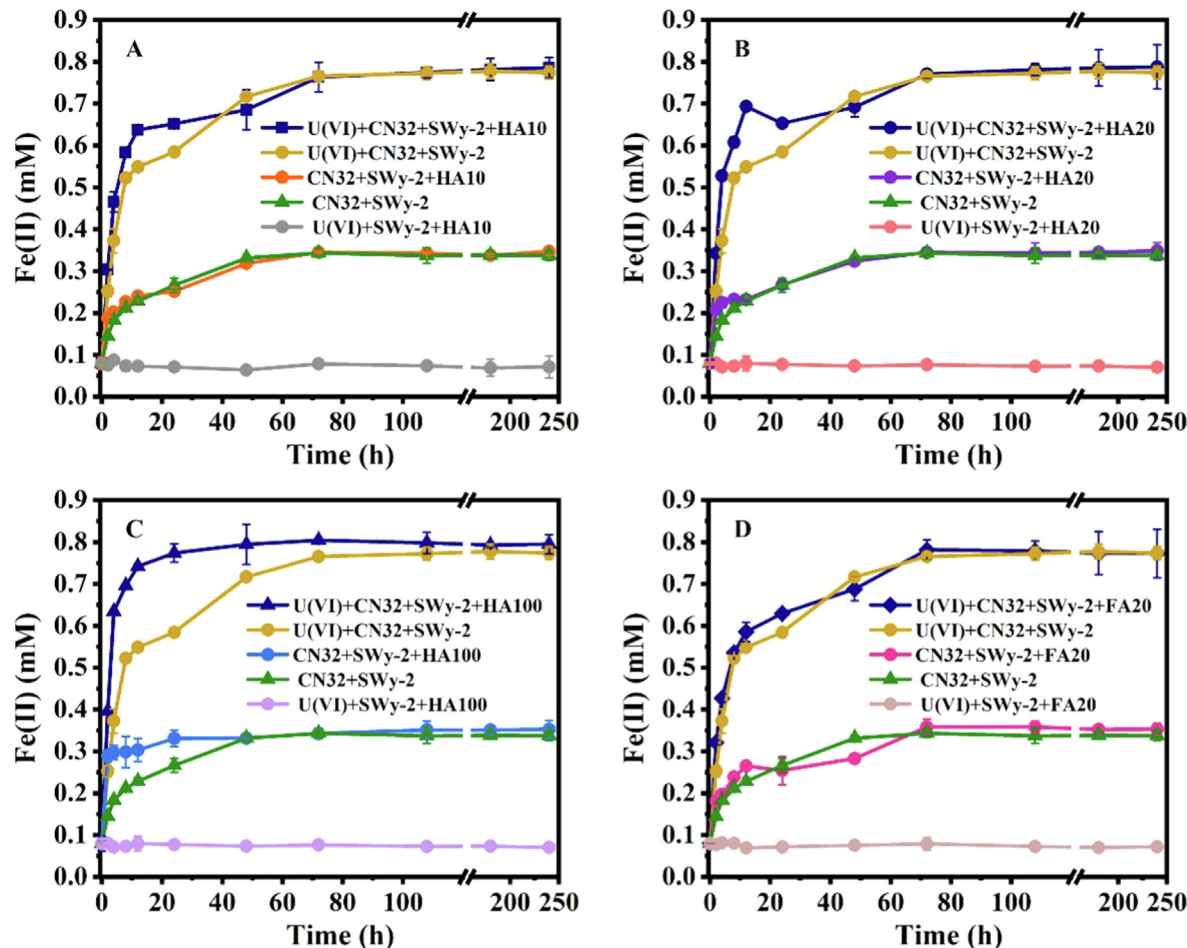


Fig. 10. Time-course increase of Fe(II) concentration in montmorillonite (SWy-2) during U(VI) bioreduction in the presence of both montmorillonite (SWy-2) and 10 ppm HA (A), 20 ppm HA (B), 100 ppm HA (C) and 20 ppm FA(D) in BP buffer (pH 7). The error bars represent one standard deviations of triplicate experiments.

Table 3
The reduction potentials (E_h) of rHA, U(VI), NAu-2, and SWy-2.

Reduction potential E_h (V)	
rHA	-0.044
U(VI)	-0.126
NAu-2	-0.037
SWy-2	+0.248

rHA denotes HA reduced by *Shewanella putrefaciens* CN32. rHA and U(VI) reduction potentials were measured in BP buffer (30 mM bicarbonate (NaHCO_3) and 10 mM PIPES solutions). U (VI) does not form any complex with HS under our experimental condition (Fig. S1). E_h of NAu-2 and SWy-2 were calculated from a reference (Luan et al., 2014).

potential than oxidized NAu-2/SWy-2 (Table 3), suggesting that electron transfer from rHA to structural Fe(III) was favorable. The other possibility is that HA dissolved some clay minerals during bioreduction (Table S3), and the resulting aqueous Fe(III)-HA/Fe(II)-HA complexes served as an electron shuttle to enhance the bioreduction of structural Fe(III) in NAu-2 (Fig. 11B), which is similar to citrate (Zhang et al., 2021). This mechanism was confirmed by a control experiment showing that HA-Fe(III) complex was reduced by CN32 and the resulting HA-Fe(II) complex reduced structural Fe(III) in NAu-2 (Fig. S2A and B), likely through a mechanism similar to interfacial electron transfer (Schaefer et al., 2011; Neumann et al., 2013). The resulting Fe(III)-HA complex could be reduced back to Fe(II)-HA complex by CN32. Therefore, the effect

of HS on Fe(III) bioreduction was a result of both direct (similar to AQDS) and indirect electron shuttling roles through formation of Fe(III)-HS/Fe(II)-HS complexes (similar to citrate).

For Fe-poor SWy-2, the enhancement of HA on Fe(III) bioreduction was weaker (Fig. 4A-C, Table S2). It was likely that less aqueous $\text{Fe}^{3+}/\text{Fe}^{2+}$ was released during bioreduction (Table S3), and the role of Fe(III)-HA/Fe(II)-HA as an electron shuttle may be limited. Compared to HA, the enhancement effect of FA was weaker for both NAu-2 and SWy-2 (Figs. 3 and 4), likely because it contains fewer redox-active moieties (Scott et al., 1998; Aeschbacher et al., 2010).

4.3. the effect of U(VI)-clay interaction on their respective bioreduction

The bioreduction rate of U(VI) was greatly inhibited in the presence of clay minerals, with Fe(III)-rich NAu-2 inhibiting more than Fe(III)-poor SWy-2 (Fig. 5A). In contrast, the presence of U(VI) showed a promoting effect on the bioreduction of structural Fe (III) in clay minerals, with a greater effect on NAu-2 than on SWy-2 (Fig. 5B). These results were consistent with those previous studies (Zhang et al., 2009; Zhang et al., 2021).

A possible mechanism (Zhang et al., 2009) was that U(VI)/U(IV) redox couple served as an electron shuttle to accelerate Fe(III) bioreduction, but in doing so, U(VI) bioreduction itself was inhibited (Fig. 11C). According to this mechanism, U(VI) was initially reduced to U(IV), but U(IV) was subsequently oxidized back to U (VI) by structural Fe(III). Therefore, it was the structural Fe(III) in clay minerals that was actually reduced, not U(VI). In other words,

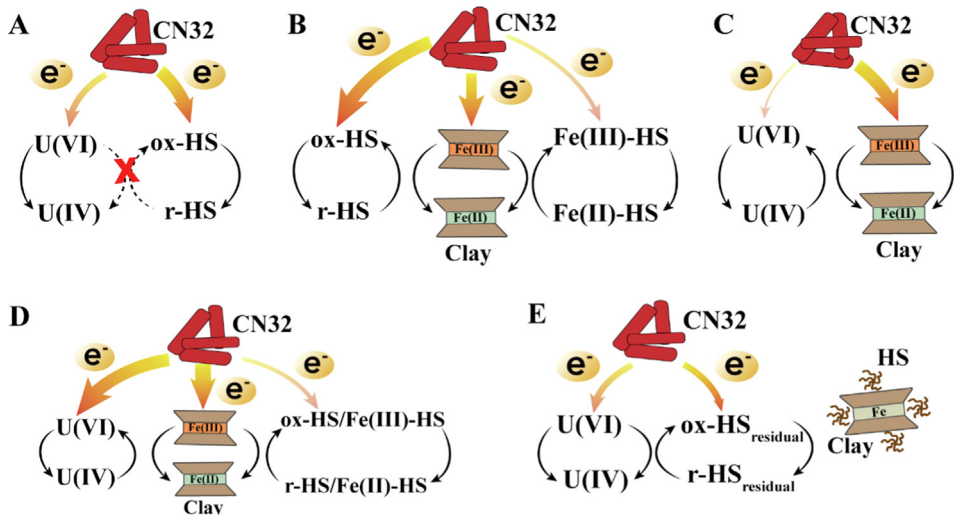


Fig. 11. Proposed reaction mechanisms for either U(VI) or Fe(III) bioreduction. Although HA and FA are separately described in the data figures and text description, a more general term HS is used in this model figure. (A) U(VI) bioreduction in the presence of humic substances (HS) by *Shewanella putrefaciens* CN32. HS retains a fraction of electrons from CN32 to U(VI) to inhibit U(VI) bioreduction. Ox-HS denotes oxidized HS, and r-HS denotes reduced HS. Because of the higher reduction potential of rHS than that of U(VI), electron transfer from rHS to U(VI) is not possible. (B) Bioreduction of structural Fe(III) in the presence of HS. HS and/or Fe(III)-HS/Fe(II)-HS redox couples serve as electron shuttles to promote electron transfer from CN32 to Fe(III) in clay minerals. (C) Bioreduction of structural Fe(III) in the presence of U(VI). U(VI)/U(IV) redox couple serves as electron shuttle to facilitate electron transfer from CN32 to structural Fe(III) in clay minerals. This mechanism inhibits U(VI) bioreduction due to electron diversion to Fe(III) but enhances Fe(III) bioreduction due to the shuttling effect of U(VI)/U(IV). (D) U(VI) bioreduction in the presence of both HS and clay minerals. U(VI)/U(IV) redox couple, HS and/or HS-Fe(III)/HS-Fe(II) redox couples all serve as electron shuttles to facilitate Fe(III) bioreduction. These interactions decrease electron diversion from U(VI) to structural Fe(III) in clays (relative to 10C) and partially alleviate their inhibitory effect on U(VI) bioreduction. (E) U(VI) bioreduction in the presence of clays and a high concentration of HS. Clays adsorb a fraction of HS and result in the compositional fractionation of HS between clay surface and the solution. The residual aqueous fraction of HS may retain fewer electrons relative to bulk HS and a fraction of those electrons may even be passed to U(VI). Therefore, clay minerals partially alleviate the inhibitory effect of HS on U(VI) bioreduction. Ox-HS_{residual} denotes the residual aqueous fraction of oxidized HS, and r-HS_{residual} denotes the residual aqueous fraction of reduced HS.

electrons were initially diverged from U(VI) to structural Fe(III) in clay minerals by the electron shuttling role of U(VI)/U(IV) redox couple, which resulted in the “lag phase” in U(VI) bioreduction kinetics (Fig. 5A). Between the two clays, SWy-2 is an Fe-poor montmorillonite, whose ability to oxidize U(IV) should be limited. Hence, the U(VI) bioreduction curve did not show the “lag phase” in the presence of SWy-2 (Fig. 5A). As bioreduction of structural Fe(III) continued, the redox potential of NAu-2 and SWy-2 would decrease (Luan et al., 2014) until a point that structural Fe(III) was no longer capable of oxidizing U(IV). From this point on, net U(VI) reduction occurred due to the presence of excess electron donor lactate. With sufficient reaction time, all U(VI) was reduced. Therefore, it was the rate of U(VI) bioreduction, not the extent, that was inhibited by clay minerals (Fig. 5A).

Previous studies showed that U(VI) could be adsorbed by clay minerals (Zhang et al., 2009; Zhang et al., 2011), which may be another reason why the presence of clay minerals impeded U(VI) bioreduction. However, only 3.28 – 6.46 % U(VI) was adsorbed to NAu-2 or SWy-2 in the absence or presence of 100 ppm HA (Fig. S4), suggesting that the effect of U(VI) adsorption on U(VI) bioreduction kinetics was limited under our experimental condition (i.e., 30 mM bicarbonate in BP buffer), consistent with a previous study (Luan et al., 2014). A previous study (Zhang et al., 2009) showed a higher extent of U(VI) adsorption (~8.5 %) when NAu-2 concentration was standardized to 2 g/L. The lower extent of U(VI) adsorption measured in this study may be because that extra 10 mM PIPES was used as a component of BP buffer, which may change the ionic strength of the electrolyte and thus impact the adsorption of U(VI) (Zhang et al., 2009).

4.4. the combined effects of HS and clay minerals on the bioreduction of U(VI)

Relative to the individual inhibitory effects of HS and clay minerals on U(VI) bioreduction, the inhibitory effect of combined HS

and clay mineral was not a simple addition of the two individual ones. Instead, it was stronger than that of HS alone, but weaker than that of clay minerals alone (Figs. 6 and 7).

Compared to clay minerals alone, addition of HS partially alleviated their inhibitory effect on U(VI) bioreduction (Figs. 6 and 7, Table 1). Therefore, addition of HS to the ternary system [U(VI) + clay + CN32] may have altered the electron transfer pathways. In the quaternary system, both HS itself and/or Fe(III)-HS/Fe(II)-HS complexes acted as electron shuttles to accelerate the reduction of structural Fe(III) in NAu-2 (Fig. 11D). In this case, structural Fe(III) in clay minerals was more rapidly reduced relative to the system without HS (Figs. 9 and 10) such that it did not have a chance to oxidize U(IV). Therefore, the ability of structural Fe(III) to divert electrons from U(VI) would be diminished, and electrons would predominantly flow to U(VI) (the thicker arrow to U(VI) in Fig. 11D than that in Fig. 11C). Therefore, it would have been this HS-mediated faster Fe(III) reduction rate that would make the inhibitory effect of clay minerals on U(VI) bioreduction less severe in the presence of HS.

In contrast to the electron-shuttling role of HS for Fe(III) bioreduction only, its analogue AQDS served as an electron shuttle for both U(VI) and structural Fe(III) in clay minerals [Fig. 2, (Zhang et al., 2009)]. Simultaneous reduction of U(VI) and Fe(III) in clays would decrease electron diversion from U(IV) to Fe(III), and therefore the rate of U(VI) reduction was much higher than that in the presence of HS. Therefore, the impact of HS on U(VI) bioreduction would be overestimated if AQDS was used as an analogue of HS.

Compared to HS alone, addition of clay minerals inhibited the initial bioreduction rate of U(VI), with NAu-2 having a greater effect than SWy-2 (Figs. 6 and 7, Table 1). The inhibitory effect of clay minerals was likely due to electron diversion (Fig. 11D), similar to that observed in the ternary system [U(VI) + CN32 + clay] (Fig. 11C). The higher Fe(III) content of NAu-2 was the likely reason for its greater inhibitory effect relative to SWy-2. However, in systems with 100 ppm HA, the U(VI) bioreduction rate was initially

slowed due to the presence of NAu-2 and SWy-2, but became faster after 4 h and 2 h, respectively (Fig. 6C and 7C). A likely reason was that the presence of clay minerals decreased the capacity of HA to retain electrons (i.e., the thinner arrow going from CN32 to oxidized HS in Fig. 11E, relative to the thicker arrow in Fig. 11A), due to adsorption-induced fractionation of HA composition. Indeed, the increased EDC and decreased EAC of the residual aqueous HA fraction relative to the bulk HA supported this scenario. Another possible reason is that residual HA may be able to shuttle electrons to U(VI) (Fig. 11E), different from the inability of original HA to perform this function (Fig. 11A). The reason for lack of such time-dependent effect at low concentrations of HS (HA/FA) may be due to negligible adsorption-induced fractionation of HS composition. In this case, there is only electron diversion effect of clay minerals. Because the compositions of AQDS and small organic acids such as citrate are much simpler than that of HS, they cannot be fractionated by adsorption to clay surface, therefore such effect was absent in the case of either AQDS or citrate.

4.5. the combined effects of HS and U(VI) on the bioreduction of Fe(III) in clay minerals

Relative to the individual enhancement effects of HS and U(VI) on Fe(III) bioreduction, the enhancement effect of combined HS and U(VI) was stronger than either one but still lower than the sum of the two. This pattern was certainly different from the combined effect of HS and clay minerals on U(VI) bioreduction.

Compared to U(VI) only, addition of HS enhanced Fe(III) bioreduction in both clays (Figs. 9 and 10, Table S2). Similar to the ternary system [Clay + CN32 + HS] (Fig. 11B), HS in the quaternary system also served as an electron shuttle to accelerate the bioreduction of structural Fe(III) (Fig. 11D). Compared with HS alone, addition of U(VI) enhanced both the initial rate and extent of Fe (III) bioreduction in NAu-2 and SWy-2 (Figs. 9 and 10, Table S2), because U(VI)/U(IV) redox couple acted as an electron shuttle between CN32 cells and Fe(III) in clay minerals. Therefore, both HS and U(VI) worked in the same direction to enhance Fe(III) bioreduction. However, the enhancement effect of combined HS and U (VI) was still lower than the sum of the two (based on the rates and extents), likely due to the limit of electron transfer rate within clay structure (Jaisi et al., 2005; Liu et al., 2017; Sheng et al., 2021) and thermodynamic constraints (Luan et al., 2014), even in the presence of multiple electron shuttles.

4.6. U(IV) speciation after bioreduction

Previous studies have demonstrated that different U(IV) species such as crystalline UO_2 (Lovley et al., 1991), non-crystalline U(IV) (Alessi et al., 2014) and aqueous ligand-complexed U(IV) (Burgos et al., 2007; Zhang et al., 2021) would form after U(VI) bioreduction under different geochemical conditions. In our study, all U(IV) was precipitated after CN32 reduction in the absence of HS and clay minerals (Table 2), which was consistent with a recent study (Zhang et al., 2021). In the presence of HA, aqueous U(IV) was formed (Table 2). U(IV) may be complexed by carboxyl and hydroxyl groups of HA (Ganesh et al., 1997) and remained in solution (Burgos et al., 2007). The ability of low concentrations of FA (20 ppm) to chelate U(IV) was apparently limited so that no soluble U(IV) was formed (Table 2).

In the presence of both clay minerals and low concentrations (10 and 20 ppm) of HS, all U(IV) was sequestered in the solid, and no aqueous U(IV) was formed (Table 2). A previous study showed that U(IV) could be adsorbed to organic carbon-coated clays (Bone et al., 2017). Although a certain amount of U(IV) was complexed with HA to form aqueous U(IV)-HA complex, after addition of NAu-2/SWy-2, U(IV) may be complexed to

HA that was adsorbed to NAu-2/SWy-2 surface. This association was supported by SEM images where C and U were co-located on the surface of NAu-2/SWy-2 (Fig. 8). However, in the quaternary systems with a high concentration of HA (100 ppm), NAu-2 and SWy-2 showed different effects (Table 2), i.e., in the presence of Fe-rich NAu-2, all U(IV) was associated with the solid, but in the presence of Fe-poor SWy-2, a fraction of U(IV) was aqueous. A similar observation was made in our previous study (Zhang et al., 2021) with EDTA, where bioreduced U(IV) was sequestered in solid and soluble U(IV)-EDTA complex in the presence of NAu-2 and SWy-2, respectively. Although NAu-2 and SWy-2 are both smectites, their different Fe contents may have caused different amounts of HA adsorption onto their surfaces, which in turn affects the ability of HA to complex with U(IV).

4.7. Environmental implications

Previous studies often used AQDS, which can serve as an electron shuttle between microbes and redox-active metals, as a simplified analogue of HS (Dong et al., 2009; Zhang et al., 2009; Meng et al., 2018). However, we found that the role of HS during U(VI) bioreduction can not be replaced by AQDS, due to their fundamental differences. HS has a higher adsorption capacity than AQDS (Gescher and Kappler, 2013). Adsorption-induced fractionation of HS composition likely changes the electron donating and accepting capacities of the residual aqueous fraction of HS. Furthermore, HS and AQDS may have different metal-chelating capacities and redox potentials (Gescher and Kappler, 2013), all of which are important in determining their effects on U(VI) bioreduction.

Some studies argued that HS may not have all the properties of natural organic matter (NOM) because they are extracted NOM (Lehmann and Kleber, 2015), other studies have shown that HS represent some of the characteristics of NOM such as electron shuttling capacity and metal chelating ability (Aeschbacher et al., 2010; Keller and Takagi, 2013; Olk et al., 2019). Therefore, our study demonstrated the importance of NOM in affecting both the complexation and redox transformation of U(VI), and thus its precipitation and mobility in soil.

The combined effects of HS and clay minerals on U(VI) bioreduction are of great importance because oxidized clay minerals are often used as nuclear waste disposal barriers (Anastácio et al., 2008; Sellin and Leupin, 2013; Grambow, 2016) and they often co-exist with HS at uranium contaminated sites (Wang et al., 2013; Bone et al., 2017; Bone et al., 2020; Fuller et al., 2020). Under these conditions, U(VI), HS, and oxidized clay minerals would interact with metal-reducing bacteria via multiple pathways. Our results showed that the interactions between HS and clay minerals not only affect the kinetics of U(VI) bioreduction, but also affect the bioreduced U(IV) speciation. From the bioreduction kinetics perspective, the combined effect of HS and Fe(III)-bearing clay minerals on U(VI) bioreduction is different from their individual effects, which expands our knowledge of uranium biogeochemistry in environmentally relevant system. From the U(IV) speciation perspective, our results demonstrated that bioreduced U(IV) would remain in solution and thus be mobile under some conditions (Fe-poor clay minerals and high concentration of HA) but may be sequestered into the solid under other conditions (Fe-rich clay minerals and low HA/FA concentration). These results suggest that it may be difficult to predict the combined effect of multiple factors on U(IV) speciation based on the individual effects of clay minerals (Boyanov et al., 2017) and organic matter (Gu et al., 2005; Burgos et al., 2007). Therefore, it is important to consider all these complexities during in-situ bioremediation and when nuclear wastes are stored using clay-rich materials.

Previous studies reported that Ca^{2+} , a common cation in the environment, may react with U(VI) and carbonate to form stable ternary Ca-U(VI)-carbonate complexes, which inhibits the bioreduction of U(VI) (Brooks et al., 2003; Belli et al., 2015). However, Ca^{2+} can be readily adsorbed by clay minerals (Cherian et al., 2018) and complexed by HS (Gu et al., 2005). Thus, the effect of Ca^{2+} on U(VI) speciation and bioreduction is expected to be small in the HS-U-clay system.

Carbonate is another important environmental factor that controls U(VI) speciation and bioreduction. In this study, we used 30 mM (bi)carbonate, an environmentally relevant concentration that was widely used in previous U(VI) bioreduction studies (Gu et al., 2005; Zhang et al., 2009; Bernier-Latmani et al., 2010; Zhang et al., 2011; Zhang et al., 2021). Our results showed that U(VI)-carbonate complexes ($\text{UO}_2(\text{CO}_3)_2^{2-}$ and $\text{UO}_2(\text{CO}_3)_3^{4-}$) were the dominant U(VI) species in the co-presence of carbonate and 100 ppm HA. The negatively charged U(VI)-carbonate complexes would impede adsorption of U(VI) to the surface of clay minerals, which may increase the bioreducibility of U(VI). Other studies showed that in the absence of carbonate, U(VI)-HA/FA complexes would form (Sachs et al., 2007), and U(VI) can be easily adsorbed to the surface of clay minerals (Chakraborty et al., 2010). Therefore, the effect of carbonate concentration on U(VI) adsorption and bioreduction in the HS-U-clay system requires further study.

5. Conclusions

Our study demonstrated that the interactions between HS and clay minerals showed a combined effect on the kinetics of U(VI) bioreduction. HS or Fe(III)-bearing clay minerals alone exhibited inhibitory effects on the bioreduction of U(VI). However, in the presence of both HS and clay minerals, the combined effect of inhibition was not a simple addition of the two individual effects. In the co-presence of clay minerals and low concentrations of HS, the combined effect of inhibition on U(VI) bioreduction was stronger than that of HS alone but weaker than that of clays alone (i.e., HS partially negated the inhibitory effect of clay minerals). In the co-presence of clay minerals and high concentration of HS, not only HS can partially negate the inhibitory effect of clay minerals on U(VI) bioreduction but also clay minerals can partially alleviate the inhibitory effect of HS on U(VI) bioreduction. In addition, the co-presence of clay minerals and HS not only affected U(VI) bioreduction kinetics, but also controlled the speciation of the reduced U(IV) product. In the presence of HA alone, aqueous U(IV) was formed. In the presence of both Fe-rich NAu-2 and HA, U(IV) was all sequestered in the solid. However, in the presence of Fe-poor SWy-2 and HA, a certain amount of U(IV) still remained in solution if the concentration of HA was high. Therefore, our study demonstrated that Fe content in clay minerals and the concentration of HS together influenced the speciation of the bioreduced U(IV). Moreover, our results demonstrated that AQDS does not fully represent the functional role of HA in the environment. U(VI) bioreduction would be overestimated if AQDS is used as an analogue of HS.

Declaration of Competing Interest

The authors declare that they have no known competing financial interests or personal relationships that could have appeared to influence the work reported in this paper.

Data availability

Data will be made available on request.

Acknowledgments

Funding for this research was provided by National Natural Science Foundation of China (No. 41630103). We thank Juan Liu from College of Environmental Sciences and Engineering of Peking University for the help of cyclic voltammetry measurements. We are grateful to Associate Editor, and three anonymous reviewers whose comments improved the quality of the manuscript.

Appendix A. Supplementary material

Supplementary material to this article can be found online at <https://doi.org/10.1016/j.gca.2022.10.026>.

References

- Aeschbacher, M., Sander, M., Schwarzenbach, R.P., 2010. Novel Electrochemical Approach to Assess the Redox Properties of Humic Substances. *Environ. Sci. Technol.* 44, 87–93.
- Aeschbacher, M., Vergari, D., Schwarzenbach, R.P., Sander, M., 2011. Electrochemical analysis of proton and electron transfer equilibria of the reducible moieties in humic acids. *Environ. Sci. Technol.* 45, 8385–8394.
- Alessi, D.S., Uster, B., Veeramani, H., Suvorova, E.I., Lezama-Pacheco, J.S., Stubbs, J.E., Bargar, J.R., Bernier-Latmani, R., 2012. Quantitative Separation of Monomeric U(IV) from UO₂ in Products of U(VI) Reduction. *Environ. Sci. Technol.* 46, 6150–6157.
- Alessi, D.S., Lezama-Pacheco, J.S., Stubbs, J.E., Janousch, M., Bargar, J.R., Persson, P., Bernier-Latmani, R., 2014. The product of microbial uranium reduction includes multiple species with U(IV)-phosphate coordination. *Geochim. Cosmochim. Acta* 131, 115–127.
- Amonette, J.E., Templeton, J.C., 1998. Improvements to the quantitative assay of nonrefractory minerals for Fe(II) and total Fe using 1,10-phenanthroline. *Clay Clay Miner.* 46, 51–62.
- Anastácio, A.S., Aouad, A., Sellin, P., Fabris, J.D., Bergaya, F., Stucki, J.W., 2008. Characterization of a redox-modified clay mineral with respect to its suitability as a barrier in radioactive waste confinement. *Appl. Clay Sci.* 39, 172–179.
- Aristilde, L., Sposito, G., 2013. Complexes of the antimicrobial ciprofloxacin with soil, peat, and aquatic humic substances. *Environ. Toxicol. Chem.* 32, 1467–1478.
- Bargar, J.R., Williams, K.H., Campbell, K.M., Long, P.E., Stubbs, J.E., Suvorova, E.I., Lezama-Pacheco, J.S., Alessi, D.S., Stylo, M., Webb, S.M., Davis, J.A., Giammar, D.E., Blue, L.Y., Bernier-Latmani, R., 2013. Uranium redox transition pathways in acetate-amended sediments. *P Natl Acad Sci USA* 110, 4506–4511.
- Belli, K.M., DiChristina, T.J., Van Cappellen, P., Taillefert, M., 2015. Effects of aqueous uranyl speciation on the kinetics of microbial uranium reduction. *Geochim. Cosmochim. Acta* 157, 109–124.
- Bernier-Latmani, R., Veeramani, H., Vecchia, E.D., Junie, P., Lezama-Pacheco, J.S., Suvorova, E.I., Sharp, J.O., Wiggin, N.S., Bargar, J.R., 2010. Non-uraninite Products of Microbial U(VI) Reduction. *Environ. Sci. Technol.* 44, 9456–9462.
- Bishop, M.E., Dong, H.L., Kukkadapu, R.K., Liu, C.X., Edelmann, R.E., 2011. Bioreduction of Fe-bearing clay minerals and their reactivity toward pertechnetate (Tc-99). *Geochim. Cosmochim. Acta* 75, 5229–5246.
- Bone, S.E., Dynes, J.J., Cliff, J., Bargar, J.R., 2017. Uranium(IV) adsorption by natural organic matter in anoxic sediments. *Proc Natl Acad Sci U S A* 114, 711–716.
- Bone, S.E., Cliff, J., Weaver, K., Takacs, C.J., Roycroft, S., Fendorf, S., Bargar, J.R., 2020. Complexation by Organic Matter Controls Uranium Mobility in Anoxic Sediments. *Environ. Sci. Technol.* 54, 1493–1502.
- Boyanov, M.I., Latta, D.E., Scherer, M.M., O'Loughlin, E.J., Kemner, K.M., 2017. Surface area effects on the reduction of UVI in the presence of synthetic montmorillonite. *Chem. Geol.* 464, 110–117.
- Brooks, S.C., Fredrickson, J.K., Carroll, S.L., Kennedy, D.W., Zachara, J.M., Plymale, A.E., Kelly, S.D., Kemner, K.M., Fendorf, S., 2003. Inhibition of bacterial U(VI) reduction by calcium. *Environ. Sci. Technol.* 37, 1850–1858.
- Burgos, W.D., Senko, J.M., Dempsey, B.A., Roden, E.E., Stone, J.J., Kemner, K.M., Kelly, S.D., 2007. Soil Humic Acid Decreases Biological Uranium(VI) Reduction by Shewanella putrefaciens CN32. *Environ. Eng. Sci.* 24, 755–761.
- Campbell, K.M., Gallegos, T.J., Landa, E.R., 2015. Biogeochemical aspects of uranium mineralization, mining, milling, and remediation. *Appl. Geochem.* 57, 206–235.
- Chakraborty, S., Favre, F., Banerjee, D., Scheinost, A.C., Mullet, M., Ehrhardt, J.J., Brendle, J., Vidal, L., Charlet, L., 2010. U(VI) Sorption and Reduction by Fe(II) Sorbed on Montmorillonite. *Environ. Sci. Technol.* 44, 3779–3785.
- Chen, J., Gu, B.H., Royer, R.A., Burgos, W.D., 2003. The roles of natural organic matter in chemical and microbial reduction of ferric iron. *Sci. Total Environ.* 307, 167–178.
- Cherian, C., Kollannur, N.J., Bandipally, S., Arnepalli, D.N., 2018. Calcium adsorption on clays: Effects of mineralogy, pore fluid chemistry and temperature. *Appl. Clay Sci.* 160, 282–289.
- Choy, C.C., Korfiatis, G.P., Meng, X., 2006. Removal of depleted uranium from contaminated soils. *J. Hazard. Mater.* 136, 53–60.
- Cui, Q., Zhang, Z., Beiyuan, J., Cui, Y., Chen, L., Chen, H., Fang, L., 2022. A critical review of uranium in the soil-plant system: Distribution, bioavailability,

- toxicity, and bioremediation strategies. *Critical Reviews in Environmental Science and Technology*, 1–26.
- Cumberland, S.A., Douglas, C., Grice, K., Moreau, J.W., 2016. Uranium mobility in organic matter-rich sediments: A review of geological and geochemical processes. *Earth Sci. Rev.* 159, 160–185.
- Dewar, D., 2019. Uranium Mining: Environmental and Human Health Effects.
- Dong, H.L., Jaisi, D.P., Kim, J., Zhang, G.X., 2009. Microbe-clay mineral interactions. *Am Mineral* 94, 1505–1519.
- El-sayed, M.E.A., Khalaf, M.M.R., Gibson, D., Rice, J.A., 2019. Assessment of clay mineral selectivity for adsorption of aliphatic/aromatic humic acid fraction. *Chem. Geol.* 511, 21–27.
- Fletcher, K.E., Boyanov, M.I., Thomas, S.H., Wu, Q., Kemner, K.M., Löffler, F.E., 2010. U (VI) Reduction to Mononuclear U(IV) by Desulfobacterium Species. *Environ. Sci. Technol.* 44, 4705–4709.
- Francis, A.J., Dodge, C.J., 2008. Bioreduction of Uranium(VI) Complexed with Citric Acid by Clostridia Affects Its Structure and Solubility. *Environ. Sci. Technol.* 42, 8277–8282.
- Fuller, A.J., Leary, P., Gray, N.D., Davies, H.S., Mosselmans, J.F.W., Cox, F., Robinson, C. H., Pittman, J.K., McCann, C.M., Muir, M., Graham, M.C., Utsunomiya, S., Bower, W.R., Morris, K., Shaw, S., Bots, P., Livens, F.R., Law, G.T.W., 2020. Organic complexation of U(VI) in reducing soils at a natural analogue site: Implications for uranium transport. *Chemosphere* 254, 126859.
- Ganesh, R., Robinson, K.G., Reed, G.D., Sayler, G.S., 1997. Reduction of hexavalent uranium from organic complexes by sulfate- and iron-reducing bacteria. *Appl Environ Microbiol* 63, 4385–4391.
- Gescher, J., Kappler, A., 2013. Microbial Metal Respiration. Springer.
- Ghosh, S., Wang, Z.Y., Kang, S., Bhowmik, P.C., Xing, B.S., 2009. Sorption and Fractionation of a Peat Derived Humic Acid by Kaolinite, Montmorillonite, and Goethite. *Pedosphere* 19, 21–30.
- Gorski, C.A., Aeschbacher, M., Soltermann, D., Voegelin, A., Baeyens, B., Marques Fernandes, M., Hofstetter, T.B., Sander, M., 2012. Redox properties of structural Fe in clay minerals. 1. Electrochemical quantification of electron-donating and -accepting capacities of smectites. *Environ. Sci. Technol.* 46, 9360–9368.
- Gorski, C.A., Klupfel, L.E., Voegelin, A., Sander, M., Hofstetter, T.B., 2013. Redox properties of structural Fe in clay minerals: 3. Relationships between smectite redox and structural properties. *Environ. Sci. Technol.* 47, 13477–13485.
- Grambow, B., 2016. Geological Disposal of Radioactive Waste in Clay. *Elements* 12, 239–245.
- Gu, B., Chen, J., 2003. Enhanced microbial reduction of Cr(VI) and U(VI) by different natural organic matter fractions. *Geochim. Cosmochim. Acta* 67, 3575–3582.
- Gu, B.H., Yan, H., Zhou, P., Watson, D.B., Park, M., Istok, J., 2005. Natural humics impact uranium bioreduction and oxidation. *Environ. Sci. Technol.* 39, 5268–5275.
- Guillaumont, R., Fanganel, T., Neck, V., Fugér, J., Palmer, D.A., Grenthe, I., Rand, M. H., 2003. Update on the chemical thermodynamics of uranium neptunium plutonium americium and technetium.
- Heitmann, T., Goldhammer, T., Beer, J., Blodau, C., 2007. Electron transfer of dissolved organic matter and its potential significance for anaerobic respiration in a northern bog. *Glob. Change Biol.* 13, 1771–1785.
- Istok, J.D., Senko, J.M., Krumholz, L.R., Watson, D., Bogle, M.A., Peacock, A., Chang, Y.-J., White, D.C., 2004. In Situ Bioreduction of Technetium and Uranium in a Nitrate-Contaminated Aquifer. *Environ. Sci. Technol.* 38, 468–475.
- Jaisi, D.P., Kukkadapu, R.K., Eberl, D.D., Dong, H., 2005. Control of Fe(III) site occupancy on the rate and extent of microbial reduction of Fe(III) in nontronite. *Geochim. Cosmochim. Acta* 69, 5429–5440.
- Keller, J.K., Takagi, K.K., 2013. Solid-phase organic matter reduction regulates anaerobic decomposition in bog soil. *Ecosphere* 4.
- Klüpfel, L., Piepenbrock, A., Kappler, A., Sander, M., 2014. Humic substances as fully regenerable electron acceptors in recurrently anoxic environments. *Nat. Geosci.* 7, 195–200.
- Kolokassidou, C., Pashalidis, I., Costa, C.N., Efstatiou, A.M., Buckau, G., 2007. Thermal stability of solid and aqueous solutions of humic acid. *Thermochim Acta* 454, 78–83.
- Lehmann, J., Kleber, M., 2015. The contentious nature of soil organic matter. *Nature* 528, 60–68.
- Lenhart, J.J., 1998. The application of surface complexation modeling to the adsorption of urinium(VI) onto hematite in the presence of humic and fulvic acids. Division of Environmental Science and Engineering, Colorado School of Mines.
- Liu, X., Dong, H., Zeng, Q., Yang, X., Zhang, D., 2019. Synergistic Effects of Reduced Nontronite and Organic Ligands on Cr(VI) Reduction. *Environ. Sci. Technol.* 53, 13732–13741.
- Liu, G., Qiu, S., Liu, B., Pu, Y., Gao, Z., Wang, J., Jin, R., Zhou, J., 2017. Microbial reduction of Fe(III)-bearing clay minerals in the presence of humic acids. *Sci. Rep.* 7.
- Long, P.E., Williams, K.H., Davis, J.A., Fox, P.M., Wilkins, M.J., Yabusaki, S.B., Fang, Y., Waichler, S.R., Berman, E.S.F., Gupta, M., Chandler, D.P., Murray, C., Peacock, A. D., Giloteaux, L., Handley, K.M., Lovley, D.R., Banfield, J.F., 2015. Bicarbonate impact on U(VI) bioreduction in a shallow alluvial aquifer. *Geochim. Cosmochim. Acta* 150, 106–124.
- Lovley, D.R., Phillips, E.J.P., Gorby, Y.A., Landa, E.R., 1991. Microbial Reduction of Uranium. *Nature* 350, 413–416.
- Lovley, D.R., Coates, J.D., BluntHarris, E.L., Phillips, E.J.P., Woodward, J.C., 1996. Humic substances as electron acceptors for microbial respiration. *Nature* 382, 445–448.
- Luan, F., Burgos, W., 2010. Bioreduction of nitrobenzene, natural organic matter and hematite by *Shewanella putrefaciens* CN32. *Geochim. Cosmochim. Acta* 74, A638–A.
- Luan, F., Gorski, C.A., Burgos, W.D., 2014. Thermodynamic Controls on the Microbial Reduction of Iron-Bearing Nontronite and Uranium. *Environ. Sci. Technol.* 48, 2750–2758.
- Luo, W., Gu, B., 2009. Dissolution and Mobilization of Uranium in a Reduced Sediment by Natural Humic Substances under Anaerobic Conditions. *Environ. Sci. Technol.* 43, 152–156.
- Luo, W., Gu, B., 2011. Dissolution of uranium-bearing minerals and mobilization of uranium by organic ligands in a biologically reduced sediment. *Environ. Sci. Technol.* 45, 2994–2999.
- Meng, Y., Zhao, Z., Burgos, W.D., Li, Y., Zhang, B., Wang, Y., Liu, W., Sun, L., Lin, L., Luan, F., 2018. Iron(III) minerals and anthraquinone-2,6-disulfonate (AQDS) synergistically enhance bioreduction of hexavalent chromium by *Shewanella oneidensis* MR-1. *Sci. Total Environ.* 640–641, 591–598.
- Mohamed, A., Yu, L., Fang, Y., Ashry, N., Riahi, Y., Uddin, I., Dai, K., Huang, Q., 2020. Iron mineral-humic acid complex enhanced Cr(VI) reduction by *Shewanella oneidensis* MR-1. *Chemosphere* 247, 125902.
- Morin, G., Mangeret, A., Othmane, G., Stetten, L., Seder-Colomina, M., Brest, J., Ona-Nguema, G., Bassot, S., Courbet, C., Guillevic, J., Thouvenot, A., Mathon, O., Proux, O., Bargar, J.R., 2016. Mononuclear U(IV) complexes and ningyoite as major uranium species in lake sediments. *Geochemical Perspectives Letters*.
- Nash, K., Fried, S., Friedman, A.M., Sullivan, J.C., 1984. Redox behavior, complexing, and adsorption of hexavalent actinides by humic acid and selected clays. *Environ. Sci. Technol.* 15, 834–837.
- Neumann, A., Olson, T.L., Scherer, M.M., 2013. Spectroscopic Evidence for Fe(II)-Fe(III) Electron Transfer at Clay Mineral Edge and Basal Sites. *Environ. Sci. Technol.* 47, 6969–6977.
- Olk, D.C., Bloom, P.R., Perdue, E.M., McKnight, D.M., Chen, Y., Farenhorst, A., Senesi, N., Chin, Y.P., Schmitt-Kopplin, P., Hertkorn, N., Harir, M., 2019. Environmental and Agricultural Relevance of Humic Fractions Extracted by Alkali from Soils and Natural Waters. *J. Environ. Qual.* 48, 217–232.
- Ratasuk, N., Nanny, M.A., 2007. Characterization and quantification of reversible redox sites in humic substances. *Environ. Sci. Technol.* 41, 7844–7850.
- Regensburg, S., Margot-Roquier, C., Harfouche, M., Froidevaux, P., Steinmann, P., Junier, P., Bernier-Latmani, R., 2010. Speciation of naturally-accumulated uranium in an organic-rich soil of an alpine region (Switzerland). *Geochim. Cosmochim. Acta* 74, 2082–2098.
- Royer, R.A., Burgos, W.D., Fisher, A.S., Jeon, B.H., Unz, R.F., Dempsey, B.A., 2002a. Enhancement of hematite bioreduction by natural organic matter. *Environ. Sci. Technol.* 36, 2897–2904.
- Royer, R.A., Burgos, W.D., Fisher, A.S., Unz, R.F., Dempsey, B.A., 2002b. Enhancement of biological reduction of hematite by electron shuttling and Fe(II) complexation. *Environ. Sci. Technol.* 36, 1939–1946.
- Sachs, S., Brendler, V., Geipel, G., 2007. Uranium(VI) complexation by humic acid under neutral pH conditions studied by laser-induced fluorescence spectroscopy. *Radiochim. Acta* 95, 103–110.
- Satpathy, A., Catalano, J.G., Giamar, D.E., 2022. Reduction of U(VI) on Chemically Reduced Montmorillonite and Surface Complexation Modeling of Adsorbed U(IV). *Environ. Sci. Technol.* 56, 4111–4120.
- Sawin, S.B., 1961. Analytical use of arsenazo III Determination of thorium, zirconium, uranium and rare earth elements. *Talanta* 8, 673–685.
- Schaefer, M.V., Gorski, C.A., Scherer, M.M., 2011. Spectroscopic evidence for interfacial Fe(II)-Fe(III) Electron Transfer in a Clay Mineral. *Environ. Sci. Technol.* 45, 540–545.
- Scott, D.T., McKnight, D.M., Blunt-Harris, E.L., Kolesar, S.E., Lovley, D.R., 1998. Quinone moieties act as electron acceptors in the reduction of humic substances by humics-reducing microorganisms. *Environ. Sci. Technol.* 32, 2984–2989.
- Sellin, P., Leupin, O.X., 2013. The Use of Clay as an Engineered Barrier in Radioactive-Waste Management – A Review. *Clay Clay Miner* 61, 477–498.
- Sharp, J.O., Lezama-Pacheco, J.S., Schofield, E.J., Junier, P., Ulrich, K.-U., Chinni, S., Veeramani, H., Margot-Roquier, C., Webb, S.M., Tebo, B.M., Giamar, D.E., Bargar, J.R., Bernier-Latmani, R., 2011. Uranium speciation and stability after reductive immobilization in aquifer sediments. *Geochim. Cosmochim. Acta* 75, 6497–6510.
- Sheng, Y., Dong, H., Kukkadapu, R.K., Ni, S., Zeng, Q., Hu, J., Coffin, E., Zhao, S., Sommer, A.J., McCarrick, R.M., Lorigan, G.A., 2021. Lignin-enhanced reduction of structural Fe(III) in nontronite: Dual roles of lignin as electron shuttle and donor. *Geochim. Cosmochim. Acta* 307, 1–21.
- Starvin, A.M., Rao, T.P., 2004. Solid phase extractive preconcentration of uranium (VI) onto diarylazobisphenol modified activated carbon. *Talanta* 63, 225–232.
- Stewart, B.D., Girardot, C., Spycher, N., Sani, R.K., Peyton, B.M., 2013. Influence of chelating agents on biogenic uraninite reoxidation by Fe(III) (Hydr)oxides. *Environ. Sci. Technol.* 47, 364–371.
- Thurman, E.M., Malcolm, R.L., 1981. Preparative isolation of aquatic humic substances. *Environ. Sci. Technol.* 15, 463–466.
- Tinnacher, R.M., Nico, P.S., Davis, J.A., Honeyman, B.D., 2013. Effects of fulvic acid on uranium(VI) sorption kinetics. *Environ. Sci. Technol.* 47, 6214–6222.
- Wang, Y., Frutschi, M., Suvorova, E., Phrommavanh, V., Descotes, M., Osman, A.A., Geipel, G., Bernier-Latmani, R., 2013. Mobile uranium(IV)-bearing colloids in a mining-impacted wetland. *Nat. Commun.* 4, 2942.
- Wang, K., Xing, B., 2005. Structural and sorption characteristics of adsorbed humic acid on clay minerals. *J. Environ. Qual.* 34, 342–349.

- Xia, Q., Zhang, L., Dong, H., Li, Z., Zhang, Y., Hu, J., Chen, H., Chen, Y., 2020. Bio-weathering of a uranium-bearing rhyolitic rock from Xiangshan uranium deposit, Southeast China. *Geochim. Cosmochim. Acta* 279, 88–106.
- Xia, Q., Jin, Q., Chen, Y., Zhang, L., Li, X., He, S., Guo, D., Liu, J., Dong, H., 2022. Combined Effects of Fe(III)-Bearing Nontronite and Organic Ligands on Biogenic U(IV) Oxidation. *Environ. Sci. Technol.* 56, 1983–1993.
- Yu, C., Zhang, Y., Lu, Y., Qian, A., Zhang, P., Cui, Y., Yuan, S., 2021. Mechanistic Insight into Humic Acid-Enhanced Hydroxyl Radical Production from Fe(II)-Bearing Clay Mineral Oxygenation. *Environ. Sci. Technol.* 55, 13366–13375.
- Zeng, Q., Dong, H., Wang, X., Yu, T., Cui, W., 2017. Degradation of 1, 4-dioxane by hydroxyl radicals produced from clay minerals. *J. Hazard. Mater.* 331, 88–98.
- Zeng, Q., Dong, H., Wang, X., 2019. Effect of ligands on the production of oxidants from oxygenation of reduced Fe-bearing clay mineral nontronite. *Geochim. Cosmochim. Acta* 251, 136–156.
- Zeng, Q., Huang, L., Ma, J., Zhu, Z., He, C., Shi, Q., Liu, W., Wang, X., Xia, Q., Dong, H., 2020a. Bio-reduction of ferrihydrite-montmorillonite-organic matter complexes: Effect of montmorillonite and fate of organic matter. *Geochim. Cosmochim. Acta* 276, 327–344.
- Zeng, Q., Wang, X., Liu, X., Huang, L., Hu, J., Chu, R., Tolic, N., Dong, H., 2020b. Mutual Interactions between Reduced Fe-Bearing Clay Minerals and Humic Acids under Dark, Oxygenated Conditions: Hydroxyl Radical Generation and Humic Acid Transformation. *Environ. Sci. Technol.* 54, 15013–15023.
- Zhang, G., Burgos, W.D., Senko, J.M., Bishop, M.E., Dong, H., Boyanov, M.I., Kemner, K.M., 2011. Microbial reduction of chlorite and uranium followed by air oxidation. *Chem. Geol.* 283, 242–250.
- Zhang, L., Luo, L., Zhang, S., 2012. Integrated investigations on the adsorption mechanisms of fulvic and humic acids on three clay minerals. *Colloids Surf., A* 406, 84–90.
- Zhang, L., Chen, Y., Xia, Q., Kemner, K.M., Shen, Y., O'Loughlin, E.J., Pan, Z., Wang, Q., Huang, Y., Dong, H., Boyanov, M.I., 2021. Combined Effects of Fe(III)-Bearing Clay Minerals and Organic Ligands on U(VI) Bioreduction and U(IV) Speciation. *Environ. Sci. Technol.* 55, 5929–5938.
- Zhang, G.X., Senko, J.M., Kelly, S.D., Tan, H., Kemner, K.M., Burgos, W.D., 2009. Microbial reduction of iron(III)-rich nontronite and uranium(VI). *Geochim. Cosmochim. Acta* 73, 3523–3538.
- Zhao, L.D., Dong, H.L., Kukkadapu, R.K., Zeng, Q., Edelmann, R.E., Pentrak, M., Agrawal, A., 2015. Biological Redox Cycling of Iron in Nontronite and Its Potential Application in Nitrate Removal. *Environ. Sci. Technol.* 49, 5493–5501.
- Zhou, P., Gu, B., 2005. Extraction of Oxidized and Reduced Forms of Uranium from Contaminated Soils Effects of Carbonate Concentration and pH. *Environ. Sci. Technol.* 39, 4435–4440.